

A SPECTROSCOPIC CATALOG OF 10 DISTANT RICH CLUSTERS OF GALAXIES

ALAN DRESSLER,¹ IAN SMAIL,^{2,3} BIANCA M. POGGIANTI,^{4,5,6} HARVEY BUTCHER,⁷
WARRICK J. COUCH,⁸ RICHARD S. ELLIS,⁴ AND AUGUSTUS OEMLER, JR.¹

Received 1998 June 12; accepted 1998 December 21

ABSTRACT

We present spectroscopic observations of galaxies in the fields of 10 distant clusters for which we have previously presented deep imaging with WFPC2 on board the *Hubble Space Telescope*. The clusters span the redshift range $z = 0.37$ – 0.56 and are the subject of a detailed ground- and space-based study to investigate the evolution of galaxies as a function of environment and epoch. The data presented here include positions, photometry, redshifts, spectral line strengths, and classifications for 657 galaxies in the fields of the 10 clusters. The catalog is composed of 424 cluster members across the 10 clusters and 233 field galaxies, with detailed morphological information from our WFPC2 images for 204 of the cluster galaxies and 71 in the field. We illustrate some basic properties of the catalog, including correlations between the morphological and spectral properties of our large sample of cluster galaxies. A direct comparison of the spectral properties of the high-redshift cluster and field populations suggests that the phenomenon of strong Balmer lines in otherwise passive galaxies (commonly called E + A but renamed here as the k + a class) shows an order-of-magnitude increase in the rich cluster environment compared with a more modest increase in the field population. This suggests that the process or processes involved in producing k + a galaxies are either substantially more effective in the cluster environment or that this environment prolongs the visibility of this phase. A more detailed analysis and modeling of these data is presented in Poggianti et al.

Subject headings: galaxies: clusters: general — galaxies: distances and redshifts — galaxies: evolution — galaxies: photometry

1. INTRODUCTION

The change with redshift observed in the proportion of star-forming galaxies in the cores of rich clusters was uncovered over 20 years ago, by Butcher & Oemler (1978, 1984), but it remains one of the clearest and most striking examples of galaxy evolution. Considerable effort has gone into acquiring photometric information that would elucidate the physical processes active in distant clusters and their effects on the evolution of both the star-forming (Lavery & Henry 1994; Lubin 1996; Rakos & Schombert 1995; Rakos, Odell, & Schombert 1997) and passive galaxies (Aragón-Salamanca et al. 1993; Stanford, Eisenhardt, & Dickinson 1995, 1998; Smail et al. 1998). Further impetus has been provided by observations of the recent transformation of the S0 population of clusters (Dressler et al. 1997), which may allow a closer connection to be drawn between the galaxy populations of distant clusters and the evolutionary signatures found in their local universe counterparts (Caldwell & Rose 1997; Bothun & Gregg 1990).

However, it was the advent of spectroscopic surveys of the distant cluster populations (e.g., Dressler & Gunn 1983, 1992, hereafter DG92; Couch & Sharples 1987, hereafter

CS87; Barger et al. 1996; Abraham et al. 1996; Fisher et al. 1998) that uncovered the real breadth of the changes in galaxies in these environments, including several spectral signatures of evolutionary change, such as evidence for a strong decline in the star formation rates of many cluster galaxies in the recent past. The advent of high-spatial resolution imaging with the *Hubble Space Telescope* (*HST*) provided a further breakthrough, giving morphological information on the galaxies in these distant clusters. This could be used to link the evolution of stellar populations in the galaxies with the evolution of their *structure* in order to understand how the various galaxy types we see in the local universe came to be. Pre- and postrefurbishment *HST* observations by two groups (Couch et al. 1994, 1998; Dressler et al. 1994; Oemler, Dressler, & Butcher 1997) were used in early attempts to correlate spectral evolution with morphological/structural data and to provide some insight into the mechanisms that might be driving the strong evolution in the cluster galaxy population. These two programs were extended from cycle 4 into the “MORPHS” project, which accumulated postrefurbishment WFPC2 images for 11 fields in 10 clusters at $z = 0.37$ – 0.56 , viewed at a time some 2 – $4 h^{-1}$ billion yr before the present day.⁹ The photometric and morphological galaxy catalogs from these images were presented in Smail et al. (1997a, hereafter S97), while the data have also been used to study the evolution of the early-type galaxies within the clusters, using both color (Ellis et al. 1997) and structural information (Barger et al. 1998), the evolution of the morphology-density relation of

¹ The Observatories of the Carnegie Institution of Washington, 813 Santa Barbara Street, Pasadena, CA 91101-1292.

² Department of Physics, University of Durham, South Rd, Durham DH1 3LE, UK.

³ Visiting Research Associate at the Carnegie Observatories.

⁴ Institute of Astronomy, Madingley Road, Cambridge CB3 0HA, UK.

⁵ Royal Greenwich Observatory, Madingley Road, Cambridge CB3 0EZ, UK.

⁶ Osservatorio Astronomico di Padova, vicolo dell'Osservatorio 5, 35122 Padova, Italy.

⁷ NFRA, PO Box 2, NL-7990, AA Dwingeloo, The Netherlands.

⁸ School of Physics, University of New South Wales, Sydney 2052, Australia.

⁹ We use $q_0 = 0.5$ and $h = H_0/100 \text{ km s}^{-1} \text{ Mpc}^{-1}$. For this geometry $1''$ is equivalent to $3.09 h^{-1} \text{ kpc}$ for our lowest redshift cluster and $3.76 h^{-1} \text{ kpc}$ for the most distant.

TABLE 1
TELESCOPE AND INSTRUMENT LOG

Telescope	Instrument	λ (\AA)	Spectral Scale (\AA pixel^{-1})	Spatial Scale (arcsec pixel $^{-1}$)	Number of Nights	Reference
Palomar 5.1 m.....	COSMIC	3500–9800	3.1	0.40	19	1
WHT 4.2 m.....	LDSS-2	3500–8300	5.3	0.59	6	2
NTT 3.5 m.....	EMMI	3600–7800	2.3	0.27	2	3

REFERENCES.—(1) Kells et al. 1999; (2) Allington-Smith et al. 1994; (3) Zijlstra et al. 1996.

the clusters (Dressler et al. 1997) and the masses of the clusters from weak lensing (Smail et al. 1997b).

The aim of this paper is to combine the morphological information available from our *HST* images with detailed star formation properties of the cluster galaxies derived from targeted spectroscopic observations. To this end we have used over 27 clear, dark nights over the past 4 years on the Palomar 5.1 m (P200),¹⁰ 4.2 m William Herschel Telescope (WHT),¹¹ and the 3.5 m New Technology Telescope (NTT)¹² to assemble a large catalog of spectroscopic data on galaxies in these clusters. We combine these new observations with previously published spectroscopy from DG92 and present spectroscopic observations of a total of 424 cluster members, of which 204 have morphologies from our *HST* imaging, as well as 233 field galaxies (71 with *HST* morphologies). In addition, we have analyzed all of the spectra, (including the DG92 spectra) to provide equivalent width (EW) measurements on a uniform system for the entire sample. The spectral catalogs, including line strength and color information, as well as the reduced spectra themselves in FITS format, are available at the AAS web site. A more detailed analysis of the spectroscopic data presented here is given in Poggianti et al. (1999, hereafter P99).

A plan of the paper follows. We start by discussing the observations and their reduction in § 2. In § 3 we then give the details of the redshift measurements, as well as our analysis to quantify the strengths of spectral features and information about our spectral classification scheme based on these. We then present the spectral properties of galaxies in the catalog and relate these to the morphologies of the galaxies from our *HST* images in § 4 before discussing our results in § 5. Finally, in § 6 we list the main conclusions of this work.

2. OBSERVATIONS AND REDUCTION

2.1. Selection of Spectroscopic Targets

The new spectroscopic observations discussed here were targeted at determining the membership of the numerous distorted and irregular galaxies revealed by our *HST* WFPC2 images of the clusters, as well as gaining a more complete understanding of the star formation properties of the general cluster population. With these aims, the object selection is closer to that employed by DG92 than the magnitude-limited selection criteria of CS87 and Barger et al. (1996). The latter approach has some claim to making

the subsequent analysis simpler, especially when the sample is selected in the near-IR. However, it is a very inefficient method for studying the faint, blue cluster members as it produces samples dominated by passive spheroidal cluster members. We chose instead to base our object selection on galaxy morphology within the region covered by our WFPC2 imaging, while being approximately magnitude-limited outside that area (selected from ground-based *r* or *i* CCD material to limits of $r \sim 22$ and $i \sim 21$). We note at this point that two of the cluster fields, A370 field 2 and Cl 0939+47 field 2, lie outside of the central regions of their respective clusters (although we do also have observations of the core regions as well). The difference in the galaxy density between the fields should be kept in mind in the following analysis, although we will highlight such selection effects for individual figures when they are discussed below. Modeling of the sample selection for the entire spectroscopic catalog is dealt with in more detail in P99.

2.2. Spectroscopic Observations

The spectroscopic observations discussed in this paper were undertaken with a variety of facilities over the period 1993–1997. We list the instruments and telescopes employed and the total number of nights used in Table 1. The basic details of the 10 clusters targeted in this study are listed in Table 2; this includes the mean cluster redshift, the one-dimensional velocity dispersion (σ_{cl} ; see § 3.2), the redshift range used to define cluster membership (Δz), the field center, and the *HST* WFPC2 filters used in the observations. The new spectra presented here are typically of high quality because of both the long exposure times employed in our observations and the combination of the high efficiency of the multiobject spectrographs and the large aperture of the telescopes used. We give in Table 3 the logs of the observing runs for the various telescopes. We list the mask identification, the dates of the observations, the total exposure time and the number of objects extracted from each mask (N). The slit width typically used was $1''.5$, with slits between $10''$ and $20''$ long. The exact size of the region on the slit used to extract the galaxy spectrum depended on the relative signal to noise of the galaxy spectrum but varied between $1''.1$ and $8''.4$ for the COSMIC spectra, with a mean length of $3''.9 \pm 1''.2$. At the median redshift of the clusters in our catalog, the spectra thus sampled a physical scale of approximately $(5 \times 13) h^{-1}$ kpc.

The exact details of the extraction and reduction of the spectra depends on the instrument and setup used. However, the basic steps were the same for all the data and we outline the procedures used for both the COSMIC and WHT/NTT data. The raw frames were debiased using the overscan regions on the chip, before being trimmed. A two-dimensional flatfield was constructed by dividing the flat-field exposure by a low-order fit in the dispersion direction.

¹⁰ The Hale 5 m telescope of the Palomar Observatory is owned and operated by the California Institute of Technology.

¹¹ The William Herschel Telescope of the Observatorio del Roque de los Muchachos, La Palma, is operated by the Royal Greenwich Observatory on behalf of the UK Particle Physics and Astronomy Council.

¹² Based in part on observations collected at the European Southern Observatory, La Silla, Chile.

TABLE 2
PROPERTIES OF THE CLUSTERS

Cluster	z	σ_{cl} (km s^{-1})	Δz	R.A. (J2000)	Decl. (J2000)	HST Filters
A 370	0.3741	1170	0.3589–0.3873	02 39 52.6	−01 34 18	F555W/F814W, F702W ^a
Cl 1447+26	0.3762	1470	0.3621–0.3857	14 49 29.3	+26 07 52	F702W
Cl 0024+16	0.3928	1150	0.3755–0.4081	00 26 35.7	+17 09 46	F450W/F814W
Cl 0939+47	0.4060	1260	0.3879–0.4173	09 42 56.1	+46 59 12	F555W/F814W, F702W ^a
Cl 0303+17	0.4184	1310	0.4018–0.4338	03 06 12.9	+17 20 08	F702W
3C 295	0.4593	1630	0.4464–0.4733	14 11 10.5	+52 12 11	F702W
Cl 0412−65	0.5074	700	0.5024–0.5130	04 12 50.1	−65 50 44	F555W/F814W
Cl 1601+42	0.5388	1210	0.5100–0.5473	16 03 12.0	+42 45 26	F702W
Cl 0016+16	0.5459	1660	0.5300–0.5601	00 18 33.3	+16 26 16	F555W/F814W ^b
Cl 0054−27	0.5608	1180	0.5520–0.5770	00 56 59.0	−27 40 20	F555W/F814W

NOTE.—Units of right ascension are hours, minutes, and seconds, and units of declination are degrees, arcminutes, and arcseconds.

^a Center (F702W), outer field (F555W/F814W).

^b Spectra from DG92.

The data frame was then divided by this normalized flat-field, this served to correct for the pixel-to-pixel response of the detector. The sequence of data frames for each mask taken on a single night were then checked for spatial offsets

between the exposures arising from flexure in the spectrograph (these are typically only $\lesssim 0.2$ pixels for COSMIC in the course of a night). If necessary the exposures were shifted in the spatial and/or dispersion direction to align

TABLE 3
LOG OF NEW SPECTROSCOPIC OBSERVATIONS

Target/Mask	Date	Exposure Time (ks)	N
COSMIC/P200			
Cl 0024+16 EW-1	1994 Aug 5–6	18.8	37
Cl 0024+16 EW-2	1994 Nov 29, 1994 Dec 1–3	20.8	34
Cl 0024+16 NS-1	1994 Oct 29–30	27.0	35
Cl 0024+16 NS-2	1995 Aug 19, 1995 Sep 25–26	20.0	29
A370 MS-1	1995 Sep 25–26	10.8	25
A370 MS-2	1995 Nov 27–28	24.0	29
A370 MS-3	1997 Oct 4	16.2	22
Cl 0303+17 EW-1	1994 Nov 29, 1994 Dec 1	25.0	30
Cl 0303+17 EW-2	1994 Dec 2	15.0	30
Cl 0303+17 NS-1	1994 Dec 3	15.0	27
Cl 0939+47 NS-B ^a	1993 Dec 13	10.8	18
Cl 0939+47 EW-B	1994 Nov 29–30, 1994 Dec 1	38.2	35
Cl 0939+47 EW-F	1994 Dec 1–2, 1995 Feb 24	36.0	34
Cl 1601+42 CM-1	1997 May 28–29	22.2	20
Cl 1601+42 CM-2	1996 Jun 18–19	21.6	22
Cl 1601+42 CM-3	1997 May 11–12, 1997 May 29	30.2	24
LDSS-2/WHT			
Cl 0939+47 WA-1	1993 Mar 24	14.4	10
Cl 0939+47 WA-2	1993 Mar 25	14.4	7
Cl 0939+47 WA-3	1993 Mar 26	10.8	7
Cl 0939+47 WA-4	1993 Mar 26	9.0	6
Cl 0939+47 MA-A,MA-D	1995 Apr 27–28	9.0	10
Cl 0939+47 MB-A,MB-D	1995 Apr 29	9.0	7
3C 295 MA-A,MA-D	1995 Apr 27	9.0	6
Cl 1447+26 WA-1	25–1993 Mar 26	10.8	23
Cl 1447+26 MA-A,MA-D	1995 Apr 28–29	12.6	9
Cl 1601+42 MA-A,MA-D	1995 Apr 28	9.0	8
EMMI/NTT			
Cl 0054−27 MA-1	1995 Nov 23	10.2	15
Cl 0054−27 MA-2	1995 Nov 24	10.8	21
Cl 0412−65 MA-1	1995 Nov 23	9.0	15
Cl 0412−65 MA-2	1995 Nov 24	8.6	21

^a Using “old” COSMIC CCD.

them and then combined with a cosmic-ray rejection algorithm using the IRAF task IMCOMBINE. This produced a two-dimensional image of the mask exposure clean of cosmic ray events. These frames were then geometrically remapped to align the spectra along the rows of the detector. This step is necessary to remove the distortion of the spectra on the detector introduced by the spectrograph optics. The distortion is only a large effect for objects in slits near the edge of COSMIC's large 13.7×13.7 field of view, although aligning the spectra also helps when tracing some of the faintest objects. The distortion of the spectra are mapped using the positions of the emission lines in the arc exposure taken after every science exposure. The positions of objects in each slit on the remapped frame, as well as regions of clear sky surrounding them, were then defined interactively using the IRAF package APEXTRACT. The exact position of the object within the slit was traced in the dispersion direction and fitted with a low-order polynomial to allow for atmospheric refraction. The spectra were then sky-subtracted and extracted using optimal weighting to produce one-dimensional spectra. The arc exposures associated with each science exposure were remapped and extracted in exactly the same manner (although with no sky subtraction) and these were used to determine the wavelength calibration for the science exposure. We estimate our wavelength scale is good to 0.2 \AA rms. Finally, the one-dimensional spectra were smoothed to the instrumental resolution, $\sim 8 \text{ \AA}$, and rebinned to $10 \text{ \AA pixel}^{-1}$ to make them more manageable. The spectra obtained with COSMIC have not been flux calibrated.

The WHT and NTT spectra have been reduced using the LEXT package, purposely written for reducing LDSS-2 spectra, and the MIDAS software package. What follows is a brief description of the reduction procedure generally adopted. A number of twilight and dome flatfields, and several arc frames were obtained for each mask, as well as numerous bias frames and long-slit spectra of standard stars for flux calibration (at least one star per night). The raw frames were first debiased and then divided by the corresponding normalized flatfield. They were then calibrated in wavelength with the arcs frames obtained either with a CuAr or HeArNe combination of lamps. The sky-subtraction step was performed with an interactive choice of the spatial limits of the spectrum, which was then extracted summing the counts weighted with a Gaussian. The long-slit stellar spectrum was reduced in a similar way as the target spectra and a response function was derived by the comparison with a tabulated spectrum. Each spectrum was flux-calibrated in F_ν by dividing for this response function. In the case of the WHT and NTT spectra each exposure of a given mask was reduced and calibrated separately, before all the spectra of a given galaxy were coadded; no smoothing or rebinning was applied.

The full digital catalog of FITS spectra collected for this program is distributed in electronic form on the AAS web site. These spectra are also available on the World Wide Web at <http://www.ociw.edu/~irs>.

3. SPECTROSCOPIC ANALYSIS

The full catalog of objects observed spectroscopically in the 10 clusters is given in Tables 4A and 4B (the complete tables are included on the AAS web site as well as being available at <http://www.ociw.edu/~irs>). This has been split into "Cluster" and "Field" samples as described below.

The tables list not only the spectral information on the galaxies, but also any available morphological and photometric data from S97 and DG92. A key to the various parameters and the format of the tables are given in Table 5. We now describe in more detail the measurement of some of the spectral parameters listed in Tables 4A and 4B.

3.1. Spectral Measurements

The quality of the spectra, both in terms of the signal-to-noise ratio and sky subtraction, was visually assessed by AD for *all* of the spectra presented. The spectra are graded on a five-point range, with $q = 1$ signifying the best and $q = 5$ the worst quality. Quality $q = 5$ spectra, approximately 10% of the sample, were rejected as not useful for identifying spectroscopic features. Of the remaining catalog 17% have $q = 1$, 47% with $q \leq 2$ and 89% are $q \leq 3$. Spectra with $q \leq 3$ have sufficient signal to noise ratio (S/N) for not only measurement of a redshift, but also to quantify the strength of any spectral features present. From the continuum regions around the $[\text{O II}] \lambda 3727$ and $\text{H}\delta$ lines we estimate median S/N of 40.2 ($q = 1$), 28.3 ($q = 2$) and 19.7 ($q = 3$), with lower limits to the S/N per pixel of 20.9, 10.6 and 4.6, respectively, for these three quality classes. Repeated observations suggest that the redshifts of $q = 1$ and $q = 2$ cases are correct at a confidence of greater than 98%, and that $q = 3$ cases are correct at a confidence of greater than 90%. In contrast, those spectra with $q = 4$ are of sufficient S/N to provide only a redshift, which may be uncertain in a significant number of cases.

Redshifts were measured from the spectra interactively using purpose-written software that compares the wavelengths of redshifted absorption and emission lines with features in the spectra. Whenever possible we used a number of features to estimate the redshift, and only in a very small number of cases is a redshift based on only a single feature: these instances are noted in the comments in Tables 4A and 4B. We list in column (24) of Tables 4A and 4B the main features used to identify the galaxy redshifts. For conciseness we have used the following abbreviations to identify the lines: Babs, Balmer absorption lines; Ha, H α ; Hb, H β ; Hd, H δ ; He, H ϵ ; H η ; Hg, H γ ; Hth, H θ ; Hz, H ζ ; G, G band; H&K, Ca H and K; Mg, Mg-B; Na, Na-D; O II, $[\text{O II}] \lambda 3727$; O III, $[\text{O III}] \lambda \lambda 4959, 5007$; bk, 4000 \AA break; Mg II, Mg II $\lambda 2799$; C III, C III $\lambda 1909$; C IV, C IV $\lambda 1549$; Fe I, Fe I $\lambda 5268$; N II, $[\text{N II}] \lambda 6583$; S II, $[\text{S II}] \lambda \lambda 6716, 6731$.

The strength of emission and absorption features in the spectra were measured using purpose-written software. The program asks the user to identify an approximate line center and depth and the average level of the straddling continuum measurements, then fits both the continuum and a gaussian profile to the feature. We give the rest frame EWs for $[\text{O II}] \lambda 3727$ and $\text{H}\delta$ in columns (5) and (6) of Tables 4A and 4B, in all instances a line seen in emission is given a negative value and is quoted in \AA . The presence and strength of these lines is used in the spectral classification scheme discussed in §3.2. If other lines in the spectrum were measurable we list their EW in the comments. We measured line strengths for not only those galaxies observed for this work, but also those from the early survey of DG92. The D4000 measurements have been similarly placed on a consistent system. These are measured using wavelength intervals as defined in Dressler & Shectman (1987). The COSMIC data share a common relation of counts to flux, approximately, but were not flux calibrated per se. A multi-

TABLE 4A
SPECTROSCOPIC CATALOG OF CLUSTER GALAXIES

Cluster (1)	ID (2)	z (3)	q (4)	[O II] (5)	H δ (6)	D4000 (7)	Class (8)	R.A. (9)	Decl. (10)	ID _{ASTR} (11)	X (12)	Y (13)	Morph. (14)	T (15)	D (16)	Int. (17)	Mag ^{a,b} (18)	Col ^{a,c} (19)	Mag ^{b,d} (20)	Col ^{b,d} (21)	Run (22)	Mask (23)	Features (24)	Comments (25)
0024	1	0.3910	4	0.0	...	2.52	k:	69.1	-64.4	294	1317	343	E	-5	0	T?	19.96	3.30	21.54	1.66	DG92	DG16
0024	2	0.3990	2	-50.2	...	1.21	e(b),CSB	97.4	11.8	871	1318	1365	Scd	6	1	I?	20.37	1.60	21.44	0.39	DG92	DG19; poss H δ str; H β emis, O III = -24
0024	3	0.3825	3	0.0	2.3	2.13	k	60.1	-15.3	739	1198	1008	Sc	5	2	I	20.12	2.56	21.01	1.10	DG92	DG59
0024	4	0.3900	4	0.0	...	2.05	k:	27.6	-15.2	573	1122	692	E	-5	1	M?	18.35	3.42	19.77	1.58	DG92	DG101
0024	5	0.3910	2	-14.4	...	1.28	e(c),e(a)	42.3	7.2	659	1373	785	Sd	7	1	...	19.97	1.95	21.30	0.76	DG92	DG104; H β = -8.3, O III = -2.9; poss Bal str; can't measure H δ
0024	6	0.3900	2	0.0	...	1.56	k	31.7	-5.5	577	1224	712	S0	-2	0	...	19.51	3.18	20.86	1.26	DG92	DG106
0024	7	0.3755	1	0.0	...	1.80	k	0.9	-44.0	403	777	497	S0/E	-3	0	...	19.35	3.32	20.66	1.45	DG92	DG112
0024	8	0.3830	3	0.0	...	1.88	k:	15.5	-14.4	461	1100	572	S0/a	0	0	I	20.08	2.88	21.49	1.38	DG92	DG120
0024	9	0.3860	3	1.85	e(c):	12.0	-16.9	460	1069	543	Sb	3	3	I/M	19.84	3.32	21.45	1.47	DG92	DG123; wk O II, O III emission?
0024	10	0.3950	1	...	3.6:	2.06	k+a/k	46.7	38.6	20.26	1.48	DG92	...	H,K,G,Mg	DG128;H δ noisy
0024	11	0.3970	3	-43.3	3.0	1.25	e(b),CSB	-26.7	-46.9	203	689	234	Sd	7	2	T	20.32	1.49	21.48	0.37	DG92	DG138; H β = -7.1, O III = -6.5
0024	12	0.3960	3	0.0	...	2.01	k:	-11.9	-24.2	304	942	327	E	-5	0	...	18.47	3.42	19.63	1.58	DG92	DG140
0024	13	0.3900	3	0.0	...	2.10	k	4.9	2.8	19.29	1.61	DG92	DG144
0024	14	0.3900	3	0.0	...	2.08	k:	0.0	0.0	343	1204	387	E	-5	0	...	18.35	3.51	19.49	1.71	DG92	DG148
0024	15	0.3956	2	0.0	...	2.02	k	-30.1	-22.7	133	914	146	S0	-2	0	...	19.94	3.32	21.10	1.42	DG92	DG175
0024	16	0.3990	2	-20.7	...	1.49	e(c):	23.9	53.6	21.34	0.84	DG92	DG177; H β = -5.6, O III*2 wk (-4.1); cannot meas H δ
0024	17	0.3902	1	-4.9	3.6	1.64	e(c)	-30.9	-18.9	127	949	128	Sbc	4	0	...	19.45	2.77	20.73	0.96	DG92	DG178 m,e
0024	18	0.3830	2	0.0	...	2.08	k:	-15.6	33.5	147	1499	158	E	-5	1	I?	19.41	3.29	20.79	1.64	DG92	DG196
0024	19	0.3940	1	-137.3	...	0.81	e(m),CSB	-70.2	-40.2	21.87	0.36	DG92	...	O III,H β ,O III	D G198; str emission; H β = -56.8, O III = -124.8
0024	20	0.3850	1	0.0	...	2.08	k:	-18.9	39.3	113	1552	114	E	-5	0	I?	18.89	3.40	19.73	1.58	DG92	DG210

NOTE.—Table 4A is published in its entirety in the electronic edition of The Astrophysical Journal. A portion is shown here for guidance regarding its form and content.

^a See S97 for more details.

^b Magnitudes are in F702W for CI 0303+17, CI 0939+47, 3C 295, CI 1447+26 and CI 1601+42, and in F814W for CI 0016+16, CI 0024+16, CI 0054-27, A 370 Field 2, CI 0412-65, CI 0939+47 Field 2.

^c WFC2 $V_{555} - I_{814}$ color information is available for: CI 0016+16, CI 0054-27, A 370 Field 2, CI 0412-65, CI 0939+47, and $B_{450} - I_{814}$ colors for CI 0024+16.

^d Aperture r -band magnitude from DG92, colors are aperture ($g-r$) measurements in all instances.

TABLE 4B
SPECTROSCOPIC CATALOG OF FIELD GALAXIES

Cluster (1)	ID (2)	z (3)	q (4)	[O II] (5)	$H\delta$ (6)	D4000 (7)	Class (8)	R.A. (9)	Decl. (10)	ID _{best} (11)	X (12)	Y (13)	Morph. (14)	T (15)	D (16)	Int. (17)	Mag ^{b,c} (18)	Col ^{b,d} (19)	Mag ₅₀ ^e (20)	Col ₆₀ ^e (21)	Run (22)	Mask (23)	Features (24)	Comments (25)
0024	108	0.1393	3	...	3.1	...	e(c)	28.9	-63.2	797	1221	1103	Sed	6	0	...	17.90	2.57	19.20	0.73	DG92	...	H α , S II	DG47; Hz = -25.5 Hz also includes [N II]? - hi excit DG220; hi excit DG290; sum of ewl_11 and ewl_7; Bal abs and no O II, but Hz = -5.4; would be k+a if Hz not accessible DG185; also H&K and break; Hz < 10 DG13; also H,K,Mg noisy spectrum, but z may be correct Hz = -29.0 DG325; sum of ewl_7 and ewl_4; v blue with mod str emission; Hz = -51.5
0024	109	0.4545	3	-12.9	0.0	1.41	e(c),CSB	-28.4	43.6	21.17	0.63	DG92	...	O II, O III H,K,Bal,Hz	
0024	110	0.2132	2	0.0	7.4	2.11	e(a)	-76.7	57.6	21.30	0.79	P9408	ewl_11		
0024	111	0.2123	3	-19.3	4.8	1.74	e(a)	-35.4	-6.3	21.97	0.84	P9408	ewl_13		
0024	112	0.4758	2	-43.8	6.5	1.54	e(a)	168.3	66.7	22.51	0.67	P9408	ewl_27		
0024	113	0.6547	4	0.0	0.0	1.80	k	228.3	43.6	P9408	ewl_32		
0024	114	0.2252	3	-22.8	4.6	1.42	e(a)	281.9	-44.8	P9408	ewl_37		
0024	115	0.2279	2	-51.8	0.0	1.46	e(b),CSB	-137.0	31.3	23.31	0.17	P9408	ewl_7		
0024	116	0.5558	2	-27.2	4.7	1.35	e(a)	-1.0	17.1	302	1371	341	Sed	-5	2	1?	20.18	2.82	P9412	ewl_15		
0024	117	0.7128	2	0.0	0.0	1.77	k+a:	133.4	15.0	22.20	1.52	P9412	ewl_26		
0024	118	0.8089	4	-15.9	0.0	1.55	e(c)	177.0	45.7	P9412	ewl_28		
0024	119	0.6569	2	-3.6	0.0	1.59	e(c)	200.6	29.9	P9412	ewl_29		
0024	120	0.6564	2	0.0	0.0	1.92	k	228.4	43.6	P9412	ewl_30		
0024	121	0.6946	2	-37.8	3.9	1.22	e(a)	246.1	32.9	P9412	ewl_32		
0024	122	0.1110	2	-35.7	4.7	2.17	e(b),CSB	-121.6	29.9	21.44	0.29	P9412	ewl_5		
0024	123	0.2153	1	0.0	0.0	1.85	k	-64.7	-254.1	P9410	ns_1		
0024	124	0.2478	2	-53.4	2.3	1.63	e(b)	-38.6	-58.7	P9410	ns_1_11		
0024	125	0.1111	2	-46.0	5.0	1.49	e(b),e(a)	-121.6	29.8	P9410	ns_1_19		
0024	126	0.2129	1	-29.5	1.3	1.81	e(c)	-57.4	38.9	19.31	0.59	P9410	ns_1_20		
0024	127	0.2724	1	0.0	0.0	1.93	e(c):	-53.9	86.8	20.40	1.27	P9410	ns_1_24		

NOTE—Table 4B is published in its entirety in the electronic edition of The Astrophysical Journal. A portion is shown here for guidance regarding its form and content.
^a See S97 for more details.
^b Magnitudes are in F702W for CI 0303+17, CI 0939+47, 3C 295, CI 1447+26 and CI 1601+42, and in F814W for CI 0016+16, CI 0024+16, CI 0054-27, A 370 Field 2, CI 0412-65, CI 0939+47 and F702W for CI 0303+17, CI 0939+47, 3C 295, CI 1447+26 and CI 1601+42, and in F814W for CI 0016+16, CI 0024+16, CI 0054-27, A 370 Field 2, CI 0412-65, CI 0939+47, and B₄₅₀-I₈₁₄ colors for CI 0024+16.

^c WFPC2 $V_{555}-I_{814}$ color information is available for: CI 0016+16, CI 0054-27, A 370 Field 2, CI 0412-65, CI 0939+47, and B₄₅₀-I₈₁₄ colors for CI 0024+16.
^d Aperture r -band magnitude from DG92, colors are aperture $(g-r)$ measurements in all instances.
^e [P/W/N] < MONTH > < YEAR >, P = Palomar 5 m, W = WHT, N = NTT, or DG92.

TABLE 5
NOTES ON THE PARAMETERS IN TABLES 4A AND 4B

Column	Parameter	Units	Format	Comment
1.....	CLUSTER		A6	Cluster
2.....	ID		I4	ID in spectroscopic catalog for cluster
3.....	z		F7.4	Redshift
			A1	Redshift quality; colon indicates questionable identification
4.....	Q		I2	Quality of spectrum: 1=High, 4=Low
5.....	[O II]	Å	F7.1	Rest frame EW of [O II] 3727
			A1	Quality of [O II] 3727 EW measurement (colon indicates questionable)
6.....	H δ	Å	F4.1	Rest frame EW of H δ , -ve indicates emission
			A1	Quality of H δ EW measurement (colon indicates questionable)
7.....	D4000		F5.2	Break strength index
8.....	CLASS		A11	Spectral classification in scheme described in § 3.3
9.....	δ RA	arcsec	F7.1	RA offset from field center in Table 2
10.....	δ Dec	arcsec	F7.1	Dec offset from field center in Table 2
11.....	ID _{HST}		I5	ID in photometric catalog for cluster ^a
12.....	X	pixels	I5	X coordinate on WFPC2 frame ^a
13.....	Y	pixels	I5	Y coordinate on WFPC2 frame ^a
14.....	MORPH		A12	Galaxy morphology ^a
15.....	T		I2	T type ^a
16.....	D		I2	Visual disturbance index ^a
17.....	INT		A6	Interpretation of disturbance ^a
18.....	MAG	Mag	F5.2	Total magnitude in F702W/F814W from WFPC2 frame ^{a,b}
19.....	COL	Mag	F5.2	Aperture color from WFPC2 frame ^{a,c}
20.....	MAG _{DG}	Mag	F6.2	Magnitude from ground-based imaging published in DG92 ^d
21.....	COL _{DG}	Mag	F6.2	Color from ground-based imaging published in DG92 ^d
22.....	RUN		A6	Code giving details of observing run ^e
23.....	MASK		A10	Mask and object slit identifier
24.....	FEATURES		A23	Spectral features identified; see § 3.1
25.....	COMMENTS		A130	Description of features in spectrum

^a See S97 for more details.

^b Magnitudes are in F702W for Cl 0303+17, Cl 0939+47, 3C 295, Cl 1447+26 and Cl 1601+42, and in F814W for Cl 0016+16, Cl 0024+16, Cl 0054-27, A 370 Field 2, Cl 0412-65, Cl 0939+47 Field 2.

^c WFPC2 $V_{555} - I_{814}$ color information is available for: Cl 0016+16, Cl 0054-27, A 370 Field 2, Cl 0412-65, Cl 0939+47, and $B_{450} - I_{814}$ colors for Cl 0024+16.

^d Aperture r -band magnitude from DG92, colors are aperture ($g-r$) measurements in all instances.

^e [P/W/N]<MONTH><YEAR>, P=Palomar 5 m, W=WHT, N=NTT, or DG92.

plicative correction of 1.34 to convert the measured D4000 to true D4000 for these data was derived by comparing the COSMIC spectra of repeated objects with the equivalent flux calibrated DG92 spectra. This procedure, although imperfect, generates reasonable and consistent results, as shown by multiple COSMIC observations of the same galaxies, which show a typical scatter of $\pm 10\%$.

We have a total of 31 repeat observations, both internally within the datasets from a single telescope, and between telescopes. We find median rms scatters of $\sigma(z_{\text{COSMIC}} - z_{\text{DG92}}) = 0.0018$ ($N = 14$), $\sigma(z_{\text{COSMIC}} - z_{\text{WHT}}) = 0.0009$ ($N = 2$) and $\sigma(z_{\text{COSMIC}} - z_{\text{COSMIC}}) = 0.0005$ ($N = 7$) for those spectra with $q \leq 3$, and no systematic offsets between any of the individual datasets: $\langle z_{\text{COSMIC}} - z_{\text{DG92}} \rangle = 0.0007$, $\langle z_{\text{COSMIC}} - z_{\text{WHT}} \rangle = -0.0009$. We therefore conclude that there are no significant offsets between the redshifts from the different datasets and hence we are confident that we can include all the observed objects in our analysis. These comparisons also show that emission-line measurements are repeatable to $\pm 5\%$. H δ measurements are good to $\pm 10\%$ above 5 Å EW, with an uncertainty that rises to about $\pm 20\%$ at 3 Å EW.

Finally, we quantified the detectability of [O II] and H δ in our spectra. This enabled us to derive the lower limits on the strength of these spectral features below which we would not have identified them. Achieving this aim was not

straightforward because the code that best measured the EWs, which is based on a gaussian line-fitting program written by Paul Schechter, does not perform well when the lines are weak or undetectable. For this reason, when we measured the strengths of features in those galaxies where the feature was not clearly seen, we by necessity had to measure EWs using the standard technique of obtaining the continuum level from straddling continuum bands, and measuring the decrement or increment in signal relative to the continuum in an interval containing the feature. We made such measurements of [O II] and H δ EW for all COSMIC spectra with qualities $q \leq 3$ of cluster members in Cl 0939+47 and Cl 0024+16, a total of 79 galaxies. The intervals are, again, as defined in Dressler & Shectman (1987). For weak, but measurable, cases the line-fitting and flux-summing techniques give equivalent results, although for strong absorption lines, in particular, the latter seems to underestimate the strength of the feature, apparently by allowing the wings of the line to lower the continuum level. We believe, however, that the two scales for measuring EWs are interchangeable for the purpose of looking for weak features.

The results of these tests are shown in Figures 1a and 1b, where we have plotted the EWs as a function of signal-to-noise ratio per pixel in the continuum bands straddling the feature. In Figure 1b we show that the galaxies that were

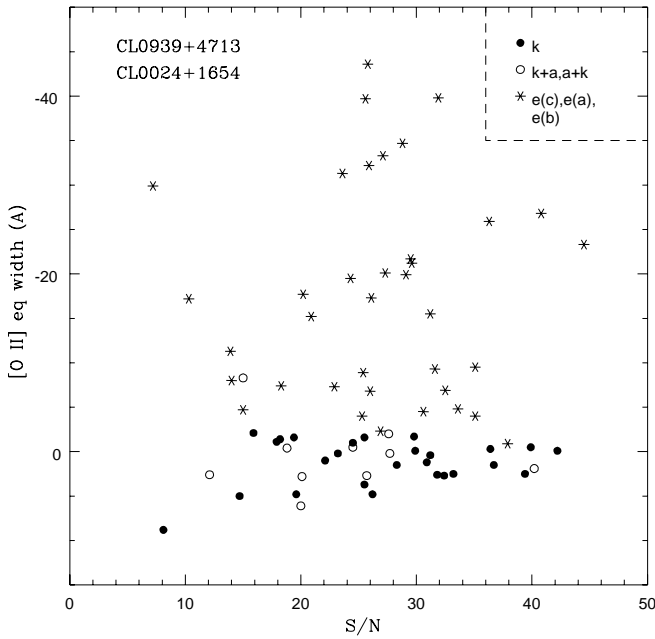


FIG. 1a

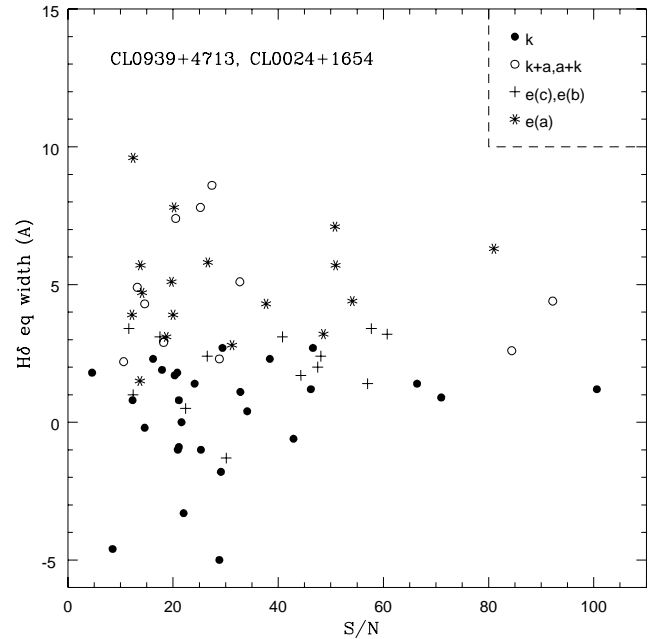


FIG. 1b

FIG. 1.—(a) Measured $[\text{O II}]$ EWs vs. the S/N in the straddling continuum. The data are for 79 cluster members with $q \leq 3$ in the clusters Cl 0939+47 and Cl 0024+16. There is a clean separation at approximately -4 \AA between the types for which $[\text{O II}]$ was found by inspection and those for which it was judged to be absent. (b) The equivalent plot for the measured $\text{H}\delta$ EWs. $\text{H}\delta$ strengths greater than 3 \AA are clear detections according to the distribution, with $2\text{--}3 \text{ \AA}$ strengths ambiguous, particularly at low S/N.

designated by inspection as emission line types all have $[\text{O II}]$ EW stronger than -3 \AA , while those designated as having no emission lines (spectral types: k, k+a, or a+k, see § 3.3) have $[\text{O II}]$ EW weaker than -4 \AA . In fact, the latter are consistent with nondetections: for 37 non-emission-line members, the median EW is $+0.4 \text{ \AA}$ with quartiles of -1.0 to $+2.6$. There is only a weak trend with signal-to-noise ratio. We conclude from these data that we are complete for $[\text{O II}]$ stronger than -5 \AA , with a high level of completeness down to -3 \AA . In other words, even at the modest signal-to-noise ratios of these spectra, none of the galaxies classified as nonemission types are likely to have emission at greater than the -3 \AA level, and certainly none have emission stronger than -5 \AA (this limit corresponds to “absent” in Table 6).

In Figure 1b we show a similar diagram for the same sample, this time for $\text{H}\delta$. Because it is weaker and in absorption, $\text{H}\delta$ is a more difficult feature to measure; this is apparent from the stronger trend with signal-to-noise ratio.

However, as for $[\text{O II}]$, the separation of those galaxies that are designated by inspection as having moderate Balmer line strengths (k+a, a+k, and e(a), see §3.3) from the non-Balmer galaxies (k and e(c) and e(b) types), is confirmed by the objective measurements. The boundary is around $2\text{--}3 \text{ \AA}$, below which point we are unable, except at high S/N (greater than 50), to discern the difference between the presence or absence of $\text{H}\delta$. We conclude from these data that we are complete above EWs of $+5 \text{ \AA}$, and mostly complete above $+3 \text{ \AA}$. It is worth commenting that some of the points with large negative EWs for $\text{H}\delta$ arise from strange continuum levels, rather than from the feature seen in emission (although there is at least one clear case of $\text{H}\delta$ in emission, a rare phenomena among luminous galaxies).

3.2. Cluster Membership

As was noted above, Table 4 is split into two parts on the basis of whether a galaxy is classed as a “Cluster” member or “Field.” To accomplish this we define redshift ranges for

TABLE 6
SPECTRAL CLASSIFICATION SCHEME

Class	EW $[\text{O II}]$ 3727 (Å)	EW $\text{H}\delta$ (Å)	Color	Comments
k.....	Absent	<3	...	Passive
k+a.....	Absent	$3\text{--}8$...	Moderate Balmer absorption without emission
a+k.....	Absent	≥ 8	...	Strong Balmer absorption without emission
e(c).....	Yes, <40	<4	...	Moderate Balmer absorption plus emission, spiral-like
e(a).....	Yes	≥ 4	...	Strong Balmer absorption plus emission
e(b).....	≥ 40	Starburst
e(n).....	AGN from broad lines or $[\text{O III}]$ 5007/ $\text{H}\beta$ ratio
e.....	Yes	?	...	With at least one emission line but S/N too low to classify
?.....	?	?	...	Unclassifiable
CSB.....	Very blue	Photometrically defined starburst

the various clusters; these ranges are purposefully chosen to be large to ensure that we retain any galaxies in the large-scale structure surrounding the clusters, while at the same time minimizing the contamination by field galaxies. In Figure 2 we show the redshift distributions for the individual cluster fields; in each panel the inset provides a more detailed view of the velocity distribution close to the cluster mean. The bin size in these plots has been arbitrarily chosen and may artificially enhance or suppress the visibility of any structures within the clusters. We list the resulting mean redshift, rest frame velocity dispersion and redshift range defining each cluster in Table 2. We reiterate that the velocity dispersions are likely to be overestimates of the true dispersion of the well-mixed cluster population. We also list in Table 2 the number of member galaxies in our catalog for each cluster. Using these definitions our catalog contains a total of 424 cluster members and 233 field galaxies.

The redshift distribution for all galaxies classed as field is shown as the open histogram in Figure 3; the galaxies with

HST morphologies are shown as the filled histogram. The median redshift of the whole field sample is $\langle z \rangle = 0.42$, while for the morphological subsample it is slightly higher at $\langle z \rangle = 0.46$ (Fig. 3). These values are very similar to the median redshift of our 10 clusters, $\langle z \rangle = 0.44$, allowing us to easily compare the broad properties of the cluster and field samples. A total of 20 stars were observed (all in either the flanking fields or from the earlier DG92 observations); these are included at the bottom of Table 4B, but we do not discuss them further.

In Figure 3 we may be seeing some evidence for a deficit in the total field redshift distribution, between $z \sim 0.4$ and 0.6 , which would result from the inclusion of a few field galaxies in the cluster catalog. This would include galaxies in the supercluster environment, if any, in which the clusters reside, or truly unassociated galaxies relatively far from the cluster but within the wide velocity limits imposed by the cluster's velocity dispersion. To estimate the extent of this effect we use two approaches. Firstly, a conservative upper

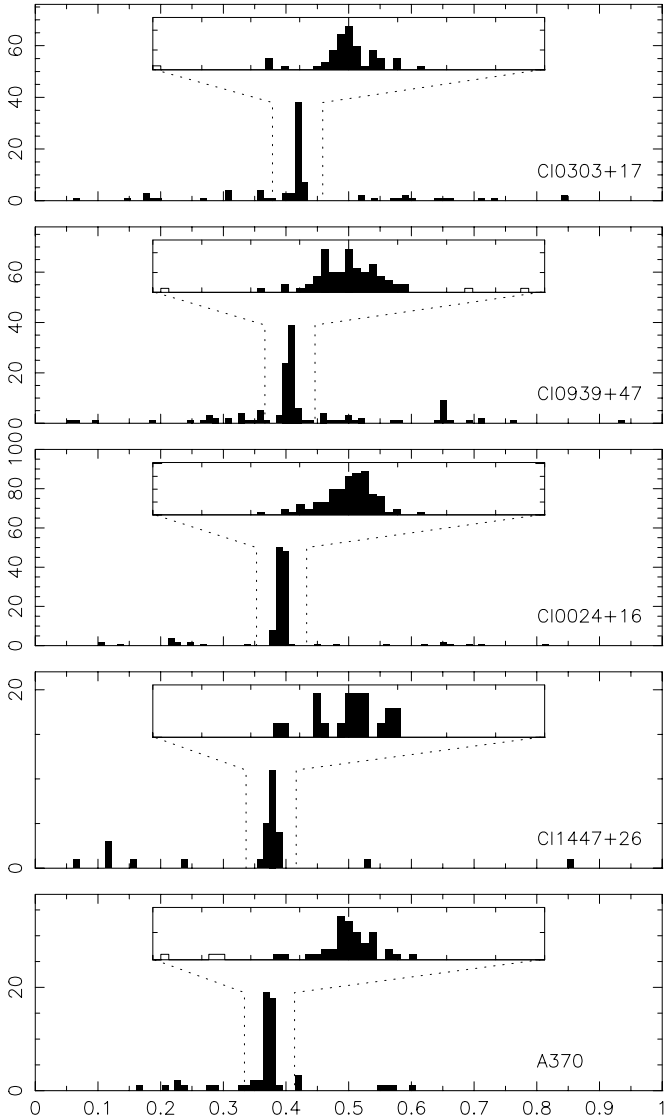


FIG. 2a

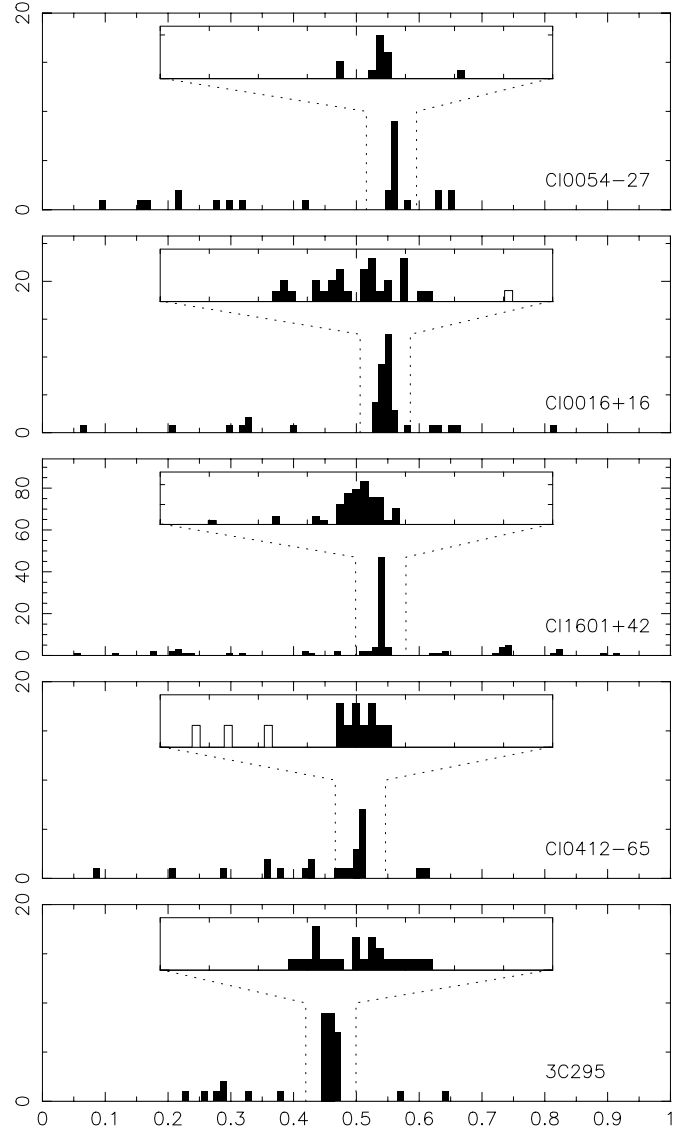


FIG. 2b

FIG. 2.—Redshift distributions for the fields of our 10 clusters. We show the redshift range $z = 0-1$ in the full plot and then, in the insets, an expanded region (width $\Delta z = 0.08$) centered on the cluster redshift. The cluster members are the filled histogram and the field galaxies open. The redshift axis in the inset panel is marked with $\Delta z = 0.01$ increments, and the vertical axis is the same as the main panel.

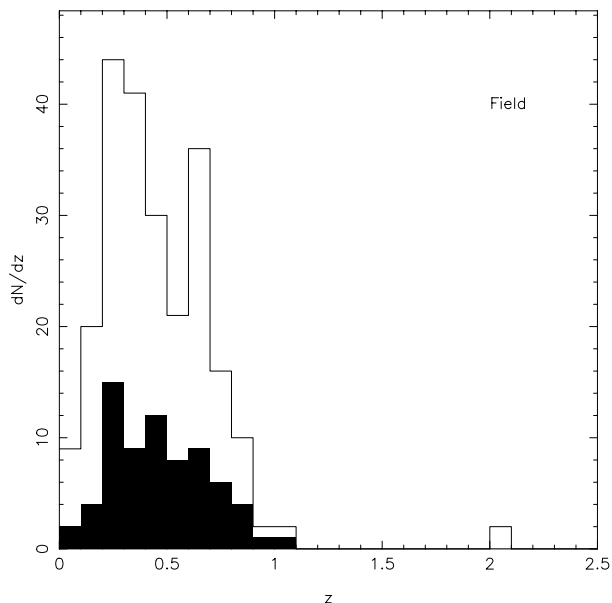


FIG. 3.—Redshift distribution for galaxies classed as nonmembers in the fields of the 10 clusters. The open histogram gives the total redshift distribution for the field galaxies (233 galaxies), and the filled histogram is for those field galaxies that lie within the WFPC2 field and for which we therefore have detailed morphological information (71 galaxies).

limit on the deficit comes from linearly extrapolating the trends of number versus redshift in the field at $z < 0.35$ and $z > 0.60$ to limit the likely number of field galaxies in the intervening redshift range. From this we estimate that there should be $\lesssim 160$ field galaxies in the range $z = 0.3-0.6$, compared with the observed number of 92, giving an upper limit on the deficit of ~ 70 galaxies, or ~ 7 per cluster. Alternatively, using the regions where the redshift limits of the cluster and field samples overlap between different clusters we estimate the contamination from random, unrelated field galaxies is of the order of 1.0 ± 0.7 galaxies per cluster in our largest velocity range. We conclude therefore that the contamination from galaxies unrelated to the cluster, or its supercluster, does not exceed 7 galaxies per cluster and is probably closer to 1–2 galaxies.

3.3. Spectral Classification

To assess the distribution in the star formation properties of galaxies in our catalog we have found it useful to classify their spectra into a number of classes. These classes are based on those used by DG92 and CS87, however, the number of classes has been expanded to better cover the full range of features seen in our large sample, and quantitative criteria are used to separate all classes. We have used the properties of low-redshift integrated spectra (Kennicutt 1992) and the expected characteristics from spectral modeling to help us define the limits of some of the classes. In revising the classifications we therefore found it necessary to redefine some of the boundaries previously used for the spectral classes. Hence, to reduce confusion between our new classes and those used previously we adopt a new nomenclature and give this and the details of the classification scheme in Table 6. We show a schematic representation of this spectral classification in Figure 4. It should be noted that for those spectra where sky residuals or the available spectral range precluded the observation of one of the diagnostic spectral features, we have made use of the

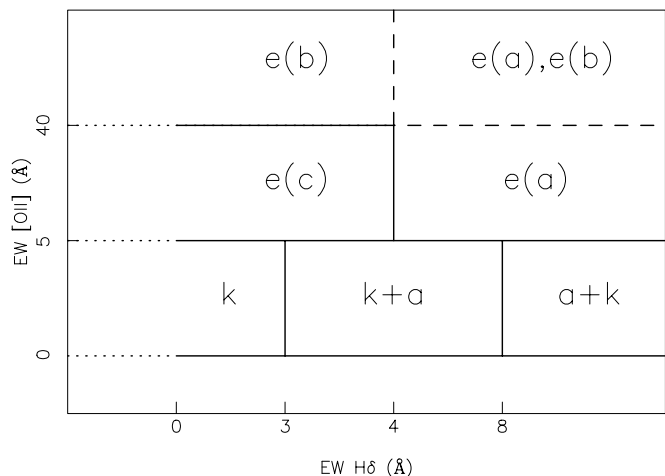


FIG. 4.—Schematic representation of the spectral classification scheme used in this work. We show the regions of the $H\delta$ - $[O\ II]$ EW plane populated by the various spectral types. Those spectral classes not based on the line strengths of $H\delta$ and $[O\ II]$ (e.g., CSB, e(n), etc.) are not marked.

strength of the other Balmer series lines (if $H\delta$ was unobservable) or emission lines (if $[O\ II]$ was unobservable) to identify the most likely spectral class. In the few cases where this has been done comments are included in Table 4.

The new system most closely resembles the DG92 system, with quantitative criteria for the new classes and subdivisions. We retain without alteration the DG92 k type. The “E + A” class is subdivided and renamed to k + a and a + k (following the suggestion of Franx 1993), depending on the strength of the $H\delta$ Balmer line. We also subdivide the DG92 e-type emission-line galaxies into e(a) types (with strong Balmer absorption), e(c) for those with weak or moderate Balmer absorption, and e(b) for those with very strong $[O\ II]$. This nomenclature reflects the nature of the spectra, with e(a) indicating a population of A stars, e(b) a spectrum similar to that expected for a burst of star formation and e(c) a spectrum for a system undergoing a more constant SFR. The reader will note the region of overlap between e(a) and e(b). Galaxies in this region have $[O\ II]$ strength corresponding to a strong burst, but also strong Balmer absorption lines that in other emission-line types are usually filled in by the Balmer emission associated with young star formation regions. The double naming reflects this ambiguity, probably because of the presence of an unusually large amount of dust. We discuss this issue further in P99.

The classification system of Couch et al. (1998, hereafter C98) is also based on based on $H\delta$ and $[O\ II]$ line strengths, but it uses $B - R$ color as well. This leads to some ambiguity when compared with the spectral classes defined in this paper. Using their sample of cluster galaxies we find that all but two of the 127 occurrences of C98’s PSV (passive) systems fall into our k class. The two remaining galaxies are classed as k/k + a. In the HDS ($H\delta$ strong) class (26 objects), again all but four fall into the k + a class and these four are classed as k + a/k. Thus, the two systems correspond very well in these classes. The PSG (poststarburst) class of C98 is defined by blue galaxies with strong $H\delta$ absorption ($EW \gtrsim 6\ \text{\AA}$) and no $[O\ II]$ emission. Of the five occurrences in our catalog, three are k + a and two are borderline a + k/k + a examples. Although C98’s class spreads over two of our general classes, the interpretation of poststarburst galaxies is consistent with our own, as discussed below. For the SB

(starburst) and Sp (spiral-like) classes of C98 the use of color as well as $[\text{O II}]$ emission leads to more mixing within our system of spectral classes. The SB class is made up of very blue galaxies with little or no $\text{H } \delta$ absorption (which is filled in by emission) and an overall weak absorption-line spectrum. Our sample has eight such occurrences, including 7 e(c) and 1 e(b) types. The Sp class is made up of blue star-forming galaxies with weak to moderately strong $\text{H } \delta$ that lie on or close to the well-defined relationship between $\text{H } \delta$ strength and color observed for local spiral galaxies by Dressler & Gunn (1983). For the 10 occurrences of such objects in our sample, four are e(c), four are e(a) and the final two are e(c)/e(a). The remaining galaxies from the sample that do not fall into our rigid interpretation of the C98 scheme include 5 red e(c) types, which have $(B-R) \geq 2$ but also show $[\text{O II}]$ emission, and 10 blue k+a and 11 blue k galaxies with no $[\text{O II}]$ emission and weak $\text{H } \delta$ but $(B-R) \leq 2$ (typically around $(B-R) \sim 1.8-2.0$, but including some examples as blue as $(B-R) \sim 1.4$). In summary, there is a general concordance of the spectral classification scheme used here and that adopted by C98, however, individual classifications for galaxies might differ slightly in their physical interpretation in the two systems. The main difference in the scheme proposed here is the distinction of the e(a) and e(c) classes in the “starforming” class of C98.

In column (8) of Table 4 we include a photometric classification in the case of the bluest galaxies. These are labeled “Color Starburst” (CSB) if their rest frame color is bluer than that expected for a low-metallicity model galaxy with an increasing star formation rate (P99). This allows us to conservatively identify those galaxies whose very blue colors can only be explained with a current starburst, whatever their spectral type may be.

To better illustrate the properties of the new classification scheme we show in Figure 5 a high-quality, representative member of each class from our catalog. In Table 7 we give the distribution of spectral classes within the different clusters (for $q \leq 4$), as well as the total numbers across all the clusters and the equivalent values for our field samples. As can be seen, the clusters are populated by a wide variety of spectral classes, although comparisons between clusters are not simple owing to the different apparent magnitudes of the samples and the attending variation in the typical quality of the spectra. Table 7 also lists the equivalent numbers of galaxies in each spectral class for which we have morphological information.

4. BASIC PROPERTIES AND CORRELATIONS OF THE DATA

To start the discussion of the spectroscopic sample we have assembled, we review the basic properties of the sample as a whole. We focus on a few of the correlations between the various properties of the galaxies in the sample, in particular the relationships between the morphological, spectral, and kinematic characteristics of certain classes of cluster galaxies. In the following discussion we will include the uncertain spectral classes (marked with a colon in Table 4), unless otherwise stated.

4.1. Luminosity Functions for the Morphological Classes

In order to draw conclusions from our spectroscopic study in the context of the broader morphological catalog (S97), we need to compare the sampling in absolute magnitude of the two catalogs. Figure 6a shows the absolute magnitude distribution for galaxies in the spectroscopic catalog

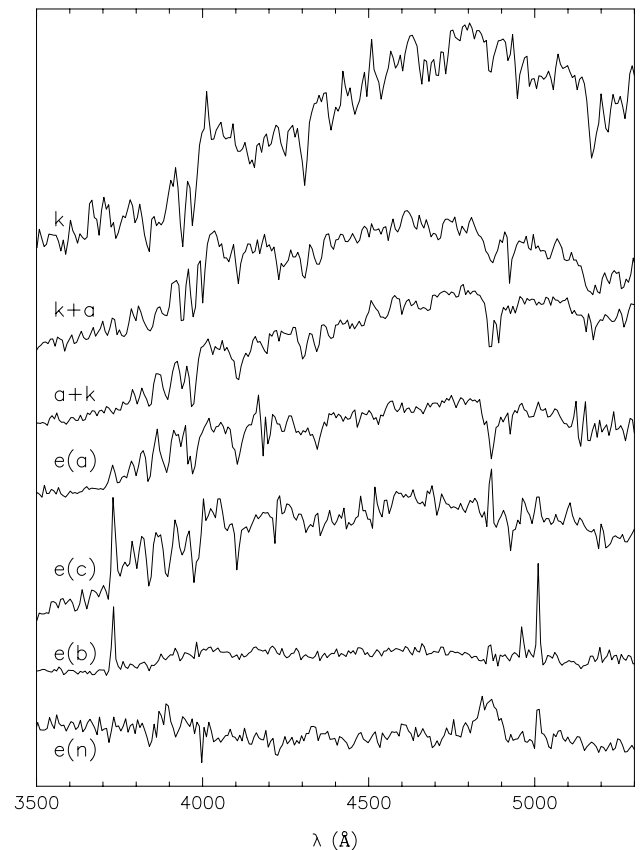


FIG. 5.—Representative spectra from each of the spectral classes in our adopted scheme (Table 6; Fig. 4). These are plotted with arbitrary vertical scaling and in the rest frame. The galaxies are all cluster members with $q = 1$ and come from Cl 0939+47 and Cl 0024+16. The spectra are not fluxed.

for which ground-based r -band photometry is available. This filter approximates V in the rest frame for all 10 clusters. Our assumption of a single K -correction (from a spectral energy distribution [SED] corresponding to a present day Sbc) introduces only small errors into the magnitude distribution ($\lesssim 0.06$ mag for E/S0 and Sd/Irr SED). Fitting a Schechter function to the bright end of the distribution in Figure 6a, we obtain a characteristic magnitude of $M_V^* = (-20.64 \pm 0.16) + 5 \log_{10} h$ (for a fixed faint-end slope of $\alpha = -1.25$ as adopted in S97). This is to be compared with a fit obtained to the morphological counts in the cluster fields corrected for likely contamination in the manner described in S97. Fitting to the composite luminosity function of all morphological types across the 10 clusters we find $M_V^* = (-20.79 \pm 0.02) + 5 \log_{10} h$ (for $\alpha = -1.25$). This good agreement indicates that the spectroscopic catalog fairly samples the morphological catalog for $M_V < -19 + 5 \log_{10} h$.

In Figure 6b we show the sampling of the spectroscopic catalog as a function of morphological type within the clusters. This is achieved by comparing the spectroscopic sample for $M_V < -19 + 5 \log_{10} h$ with the field-corrected morphological counts of S97. There is no significant trend with morphological type except for the selection effect, discussed in § 2.1, built into the original sample selection: the Sd/Irregular galaxies are oversampled relative to the E–Sc types (although there is considerable uncertainty in the statistical correction for field galaxies in this bin, S97). This

TABLE 7
SPECTRAL SAMPLES

Cluster	N_{tot}	k	k+a	a+k	e(a)	e(c)	e(b)	e(n)	e	?
Full Sample										
Field	233	36	7	0	37	74	39	3	25	12
A 370	40	26	1	0	3	8	1	0	0	1
Cl 1447+26.....	21	7	1	0	6	6	1	0	0	0
Cl 0024+16.....	107	47	12	2	13	21	6	2	2	2
Cl 0939+47.....	71	31	13	6	7	10	2	1	1	0
Cl 0303+17.....	51	14	4	4	6	12	6	0	5	0
3C 295.....	25	10	6	1	2	2	0	3	1	0
Cl 0412-65.....	10	0	1	0	0	0	1	0	1	7
Cl 1601+42.....	58	33	15	0	4	3	2	1	0	0
Cl 0016+16.....	29	13	6	5	3	1	1	0	0	0
Cl 0054-27.....	12	5	1	0	0	1	0	0	3	2
Total.....	424	186	60	18	44	64	20	7	13	12
Morphological Sample										
Field	71	11	5	0	7	25	11	0	9	3
A 370	14	9	0	0	2	1	1	0	0	1
Cl 1447+26.....	10	4	0	0	2	3	1	0	0	0
Cl 0024+16.....	42	25	6	0	4	3	3	0	1	0
Cl 0939+47.....	31	16	6	2	5	2	0	0	0	0
Cl 0303+17.....	28	9	2	3	4	5	4	0	1	0
3C 295.....	20	7	5	0	2	2	0	3	1	0
Cl 0412-65.....	2	0	0	0	0	0	0	0	0	2
Cl 1601+42.....	28	20	5	0	0	1	1	1	0	0
Cl 0016+16.....	22	10	4	5	2	1	0	0	0	0
Cl 0054-27.....	7	4	0	0	0	0	0	0	1	2
Total.....	204	104	28	10	21	18	10	4	4	5

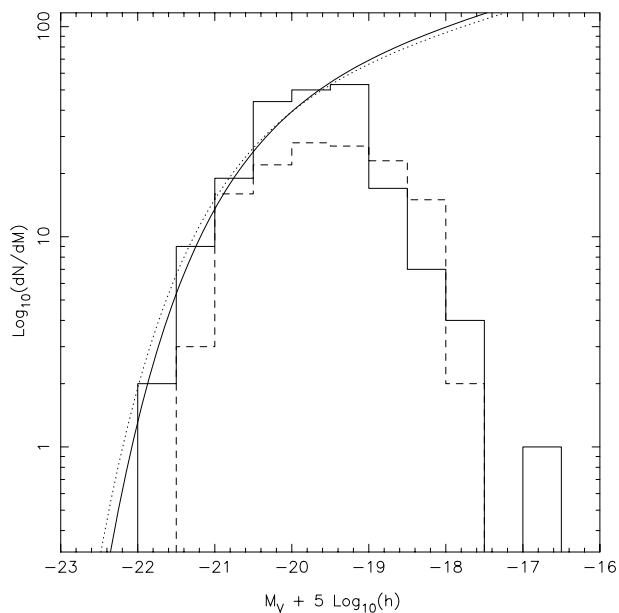


FIG. 6a

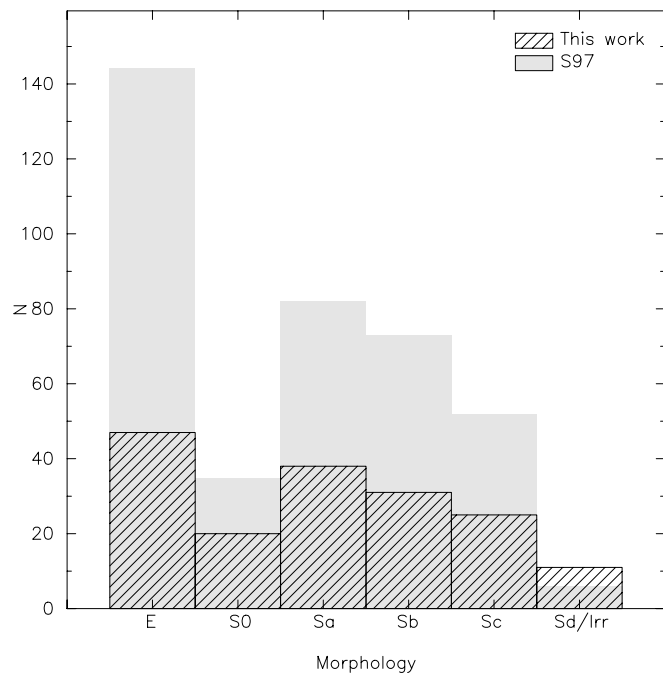


FIG. 6b

FIG. 6.—(a) Absolute magnitude distribution, in the rest frame V band, for the spectroscopic sample of cluster (*solid histogram*) and field (*dashed histogram*) galaxies (for those galaxies with DG92 photometry). The solid curve is the best-fit Schechter function to the cluster members using a fixed faint-end slope of $\alpha = -1.25$. The characteristic luminosity derived from the fit is $M_V^* = -20.64 \pm 0.16 + 5 \log_{10} h$. The dotted line shows the fit to the luminosity functions derived from the morphological counts in the frames corrected for field contamination (S97). This fit is shown for $\alpha = -1.25$ and with arbitrary vertical scaling. The good agreement of the two distributions shows that the spectroscopic catalog provides a representative luminosity distribution in the clusters at $M_V < -19 + 5 \log_{10} h$. (b) The numbers of the different morphological types in the spectroscopic catalog (*hatched histogram*) brighter than $M_V = -19 + 5 \log_{10} h$ are shown. The filled histogram indicates the total numbers expected from the observed morphological counts in the clusters to the same depth after correcting for field contamination (see S97).

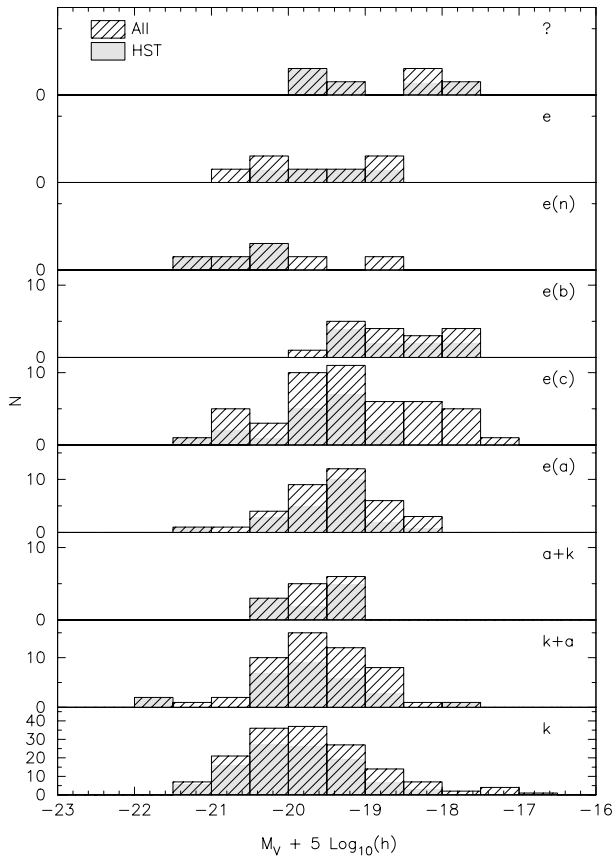


FIG. 7a

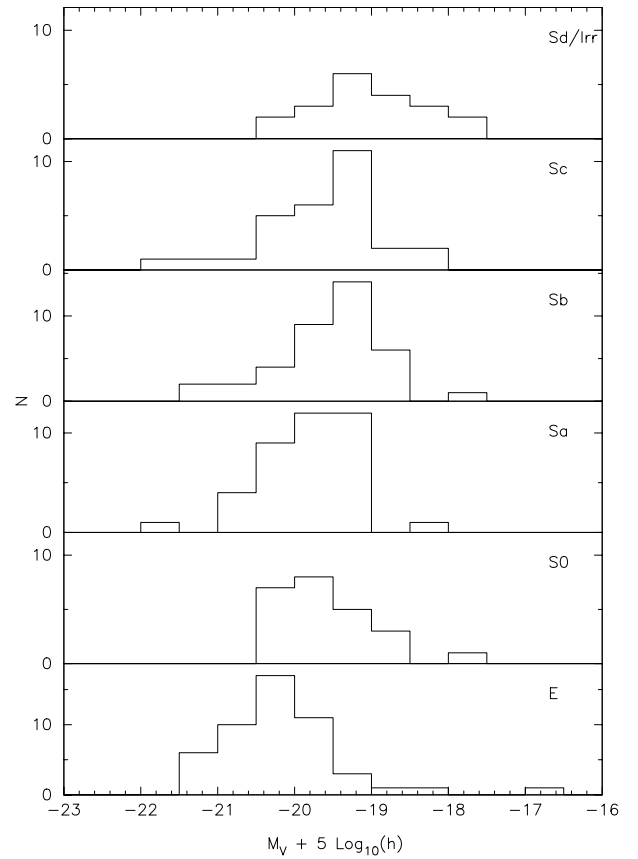


FIG. 7b

FIG. 7.—(a) Absolute magnitude distribution in the rest frame V band for cluster members separated into the different spectroscopic classes for both the HST fields and the full sample. In this panel we convert the ground-based r -band photometry to rest frame V band. (b) The same distribution but now separated on morphological type and using the HST photometry. The K -correction applied in both cases assumes an SED similar to a local Sbc galaxy, this introduce a typical systematic error of only ~ 0.06 mag for E/S0 and Sd/Irr SEDs. In both figures the nominal completeness limit is $M_V = -19 + 5 \log_{10} h$.

plot allows us to quantify and correct for the sample selection in our analysis as required.

4.2. Luminosity Functions for the Spectral Classes

The absolute magnitude distribution of the spectral classes defined in this paper will be important for understanding their relationships within the framework of galaxy evolution models. Figure 7a shows that the magnitude distributions brighter than $M_V = -19 + 5 \log_{10} h$ for spectral classes k, k+a and a+k are statistically indistinguishable. In contrast, the e(a) and e(c) classes appear to be systematically fainter than the k class; this difference is confirmed at the $\geq 95\%$ confidence limit using two-sample Kolmogorov-Smirnov tests. It is important to keep in mind the “completeness” limit of the spectroscopic catalog estimated in §4.1, which means that these differences could be larger, and, for example, the apparent peak in the luminosity distribution of e(a)’s in Figure 7a may be partly an artifact of incomplete sampling. The difference between the k class and the fainter e(b) class is clearly significant: the likelihood that the two samples are drawn from the same luminosity distribution is only $\log_{10} P \sim -4.6$. Again, the difference may be larger still, owing to the incomplete sampling below ($M_V = -19 + 5 \log_{10} h$). We know of no selection effect in our study that would cause us to miss bright e(b) cluster galaxies. As we discuss in P99, the fact that the galaxies that we have identified as bursting are fainter than the other classes is significant, and discouraging for models that

attempt to interpret these starbursts as progenitors for galaxies with strong Balmer lines in their spectra.

The cluster sample defined by our redshift measurements also allow us to unambiguously derive, for the first time, the absolute magnitude distributions as a function of morphology, again for $M_V \leq -19 + 5 \log_{10} h$. Figure 7b shows a broad similarity between the absolute magnitudes of early- and midtype disk systems (S0–Sa–Sb–Sc). Compared with these, elliptical galaxies show a systematically brighter distribution, and irregular galaxies exhibit a tail of fainter systems. These trends are in good agreement with what is seen in low-redshift populations.

4.3. Morphological Properties of the Cluster Galaxies

What do the galaxies in our spectral classes look like? We illustrate the morphologies of the cluster members within each spectral class in Figure 8. The general trend toward later types in the active spectral classes is clear. The passive spectral classes are dominated by early-type galaxies, particularly ellipticals. The correspondence of morphology and spectral properties, the same as found for low-redshift analogs, indicates that a substantial fraction of the luminous ellipticals of these clusters was in place by $z \sim 0.5$ (Ellis et al. 1997; Dressler et al. 1997). The e(c) spectra are generally associated with disk galaxies, most of them familiar spirals and irregulars. This is true of some of the e(a)’s as well, but this class also includes many disk systems that look more disturbed than typical present-day

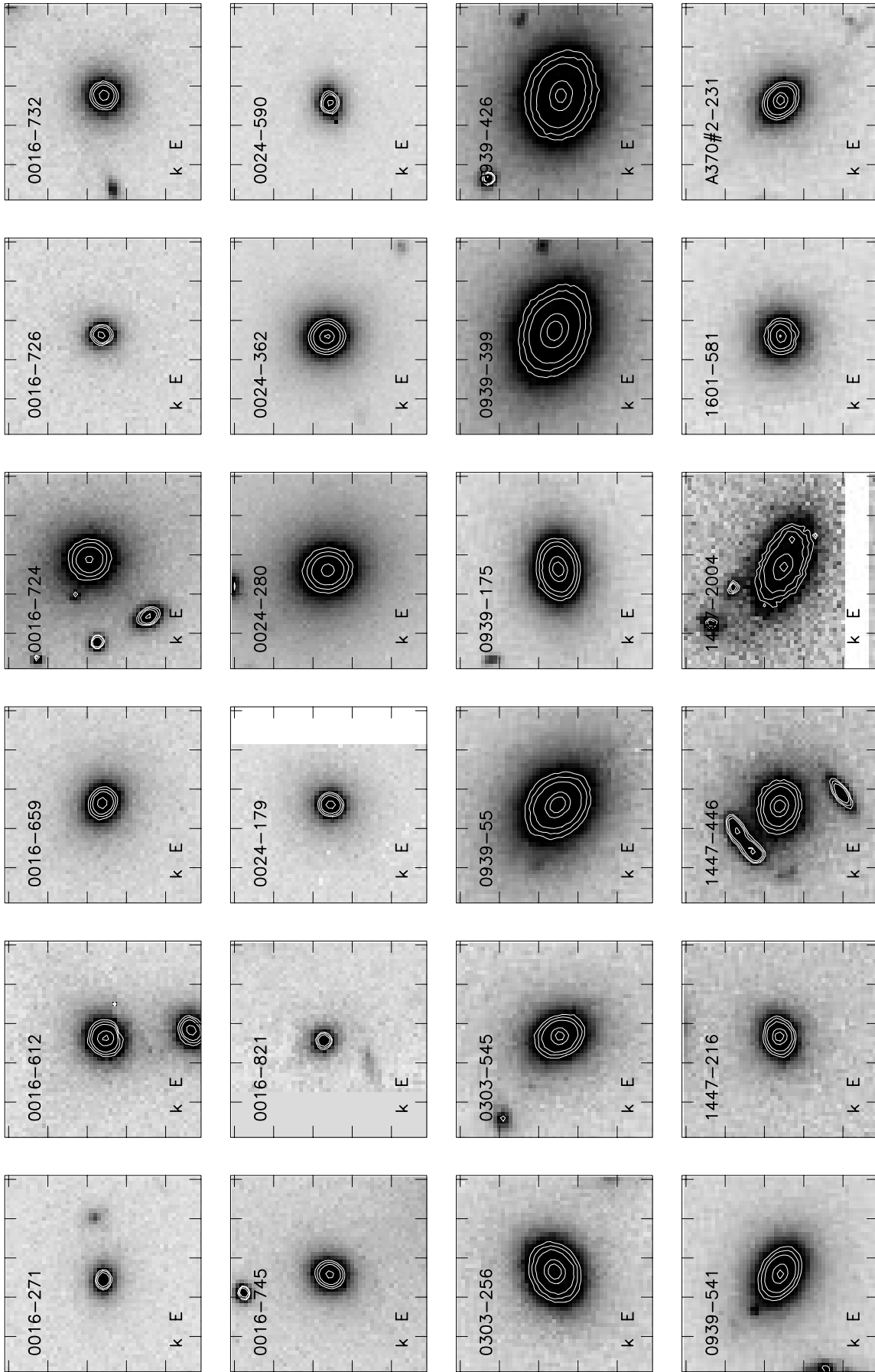


FIG. 8a

FIG. 8.—(a) Images of those galaxies in our sample lying within the WFC2 frame, grouped into spectroscopic classes. This first panel shows those galaxies with k spectral types. Each image is $5'' \times 5''$ (or $15.5\text{--}18.6 h^{-1} \text{ kpc}$ depending on the cluster's redshift) and has the same orientation as the *HST* field (S97). The cluster and galaxy ID from the WFC2 catalogs (from Table 4 in S97 or Table 4A below) and the spectral class and morphological type are marked on each frame. (b) The $k + a$ sample. (c) The $k + k$ sample. (d) The $k + a + k$ sample. (e) The $e(c)$ sample. (f) The $e(b)$ sample. (g) The $e(n)$ sample.

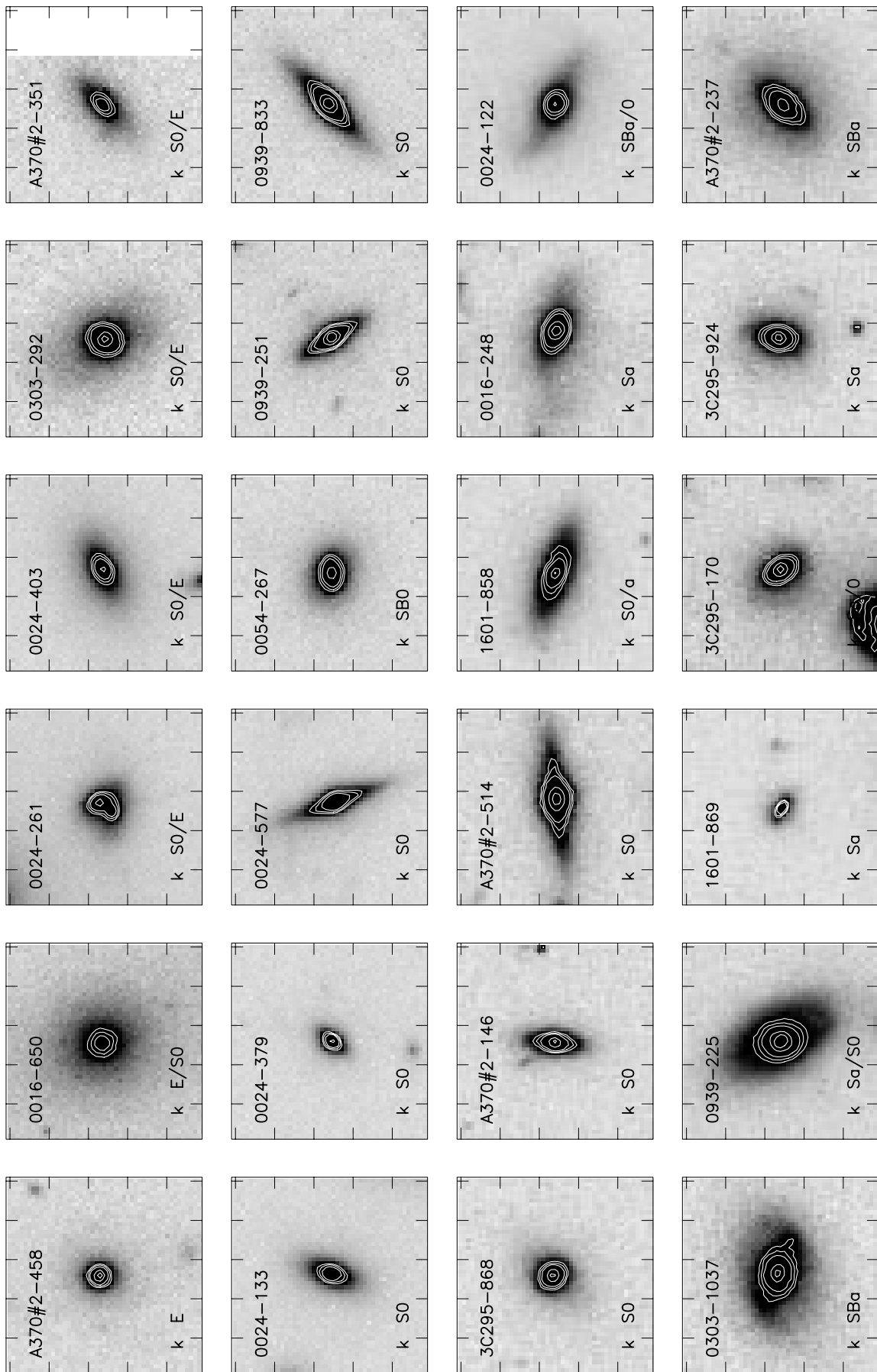


FIG. 8b

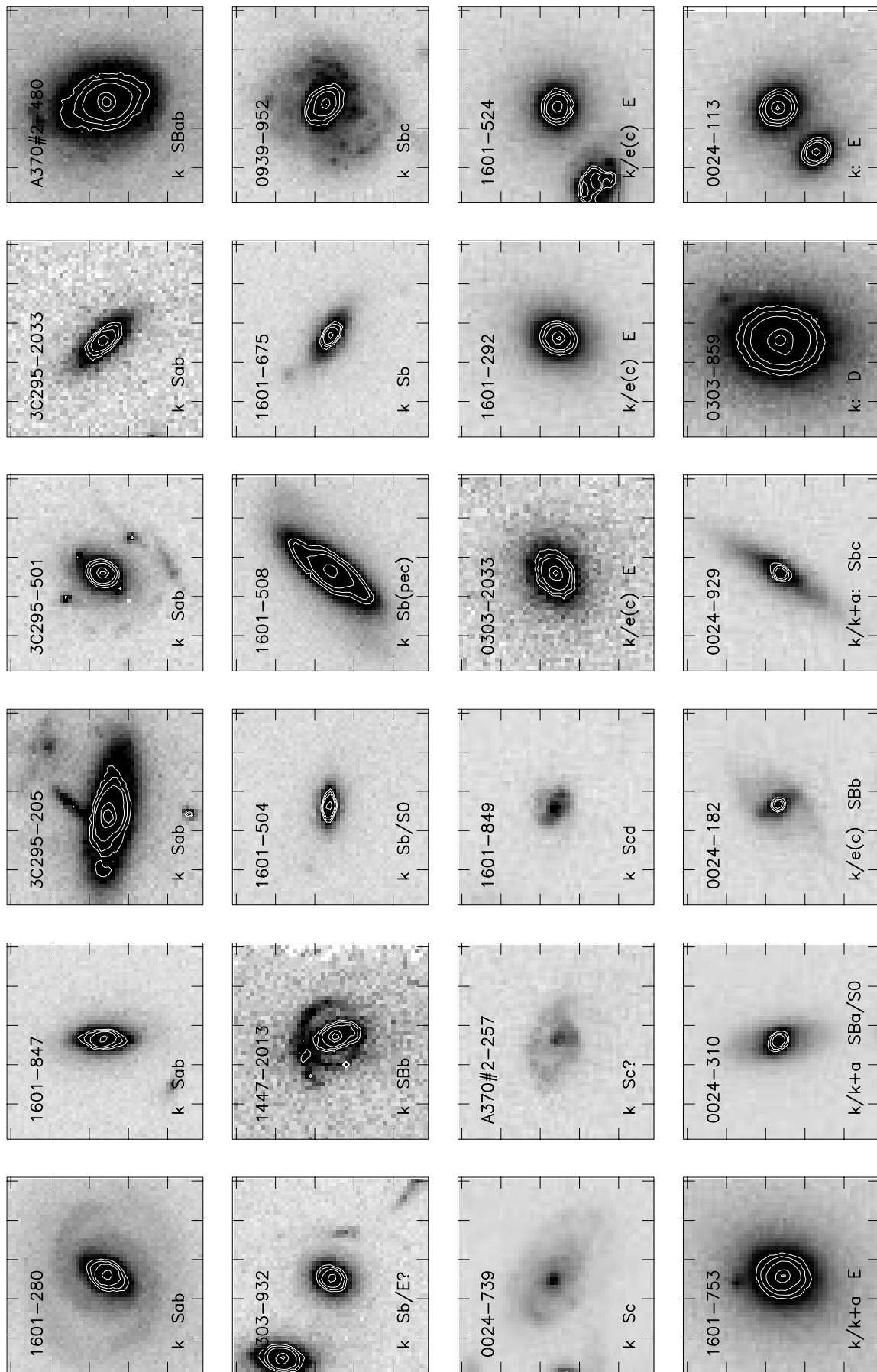


FIG. 8c

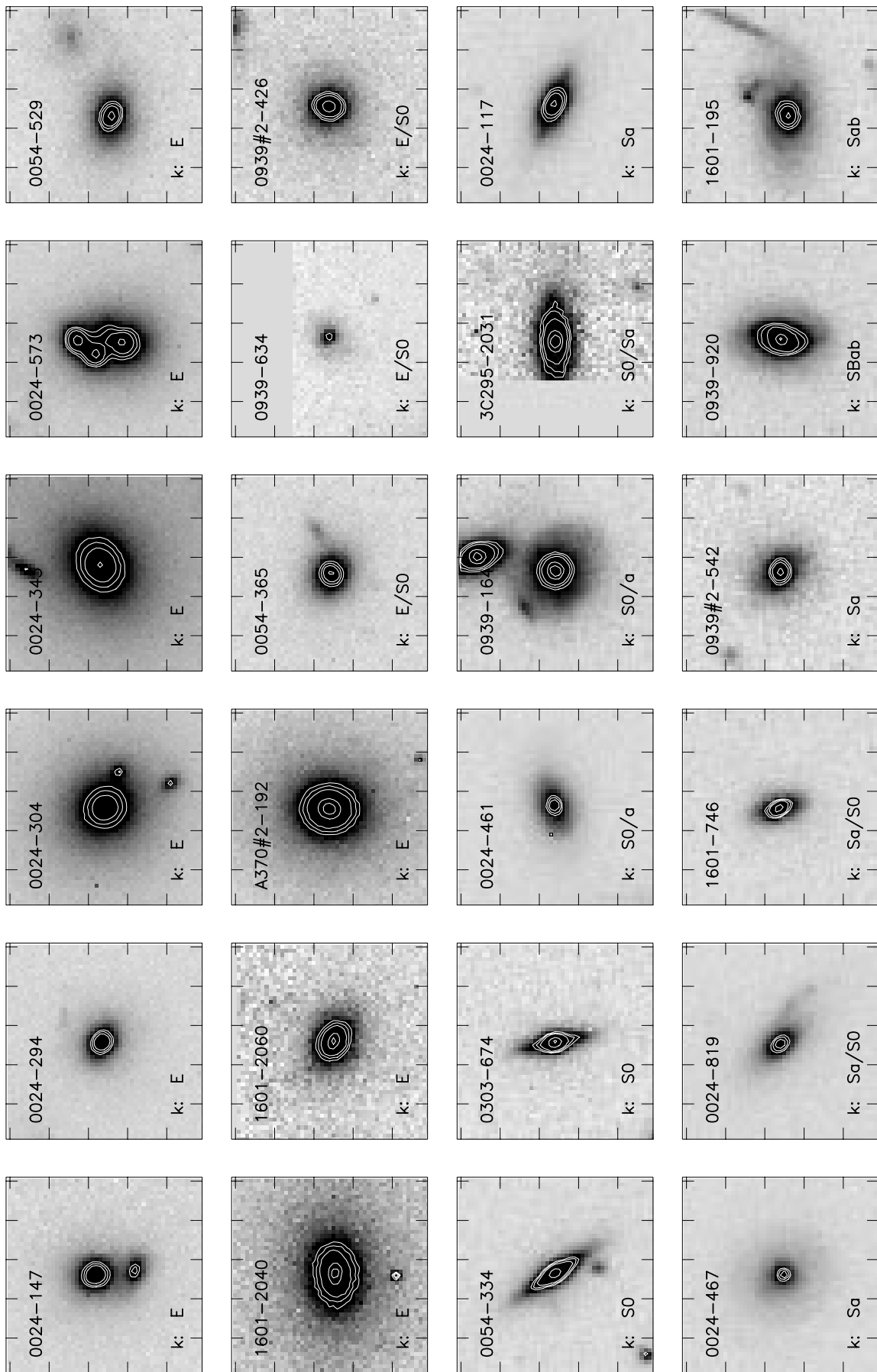


FIG. 8d

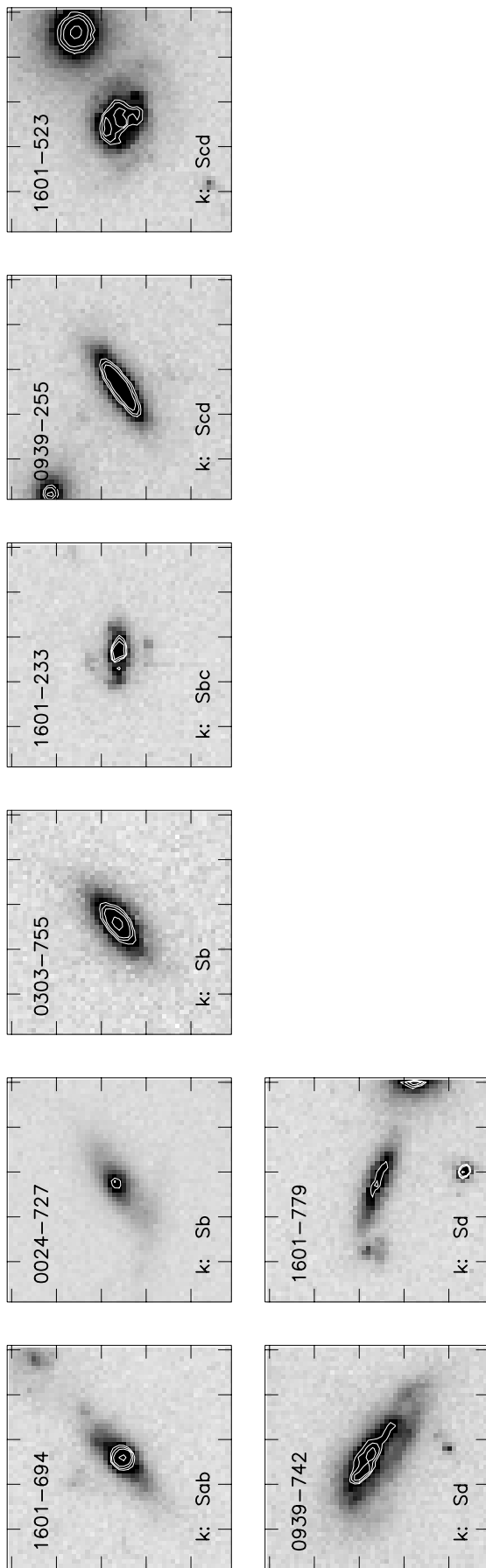


FIG. 8e

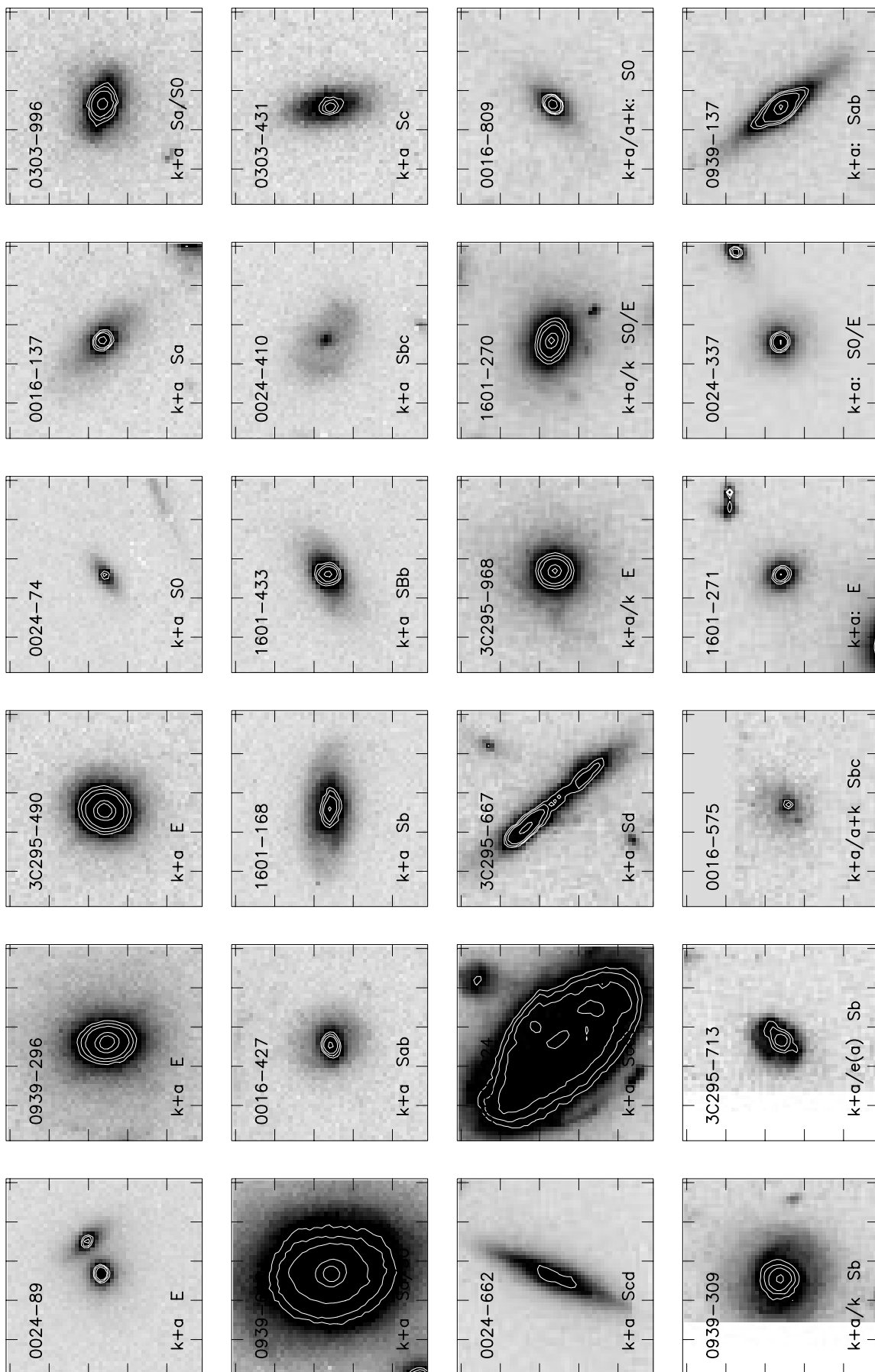


FIG. 8f

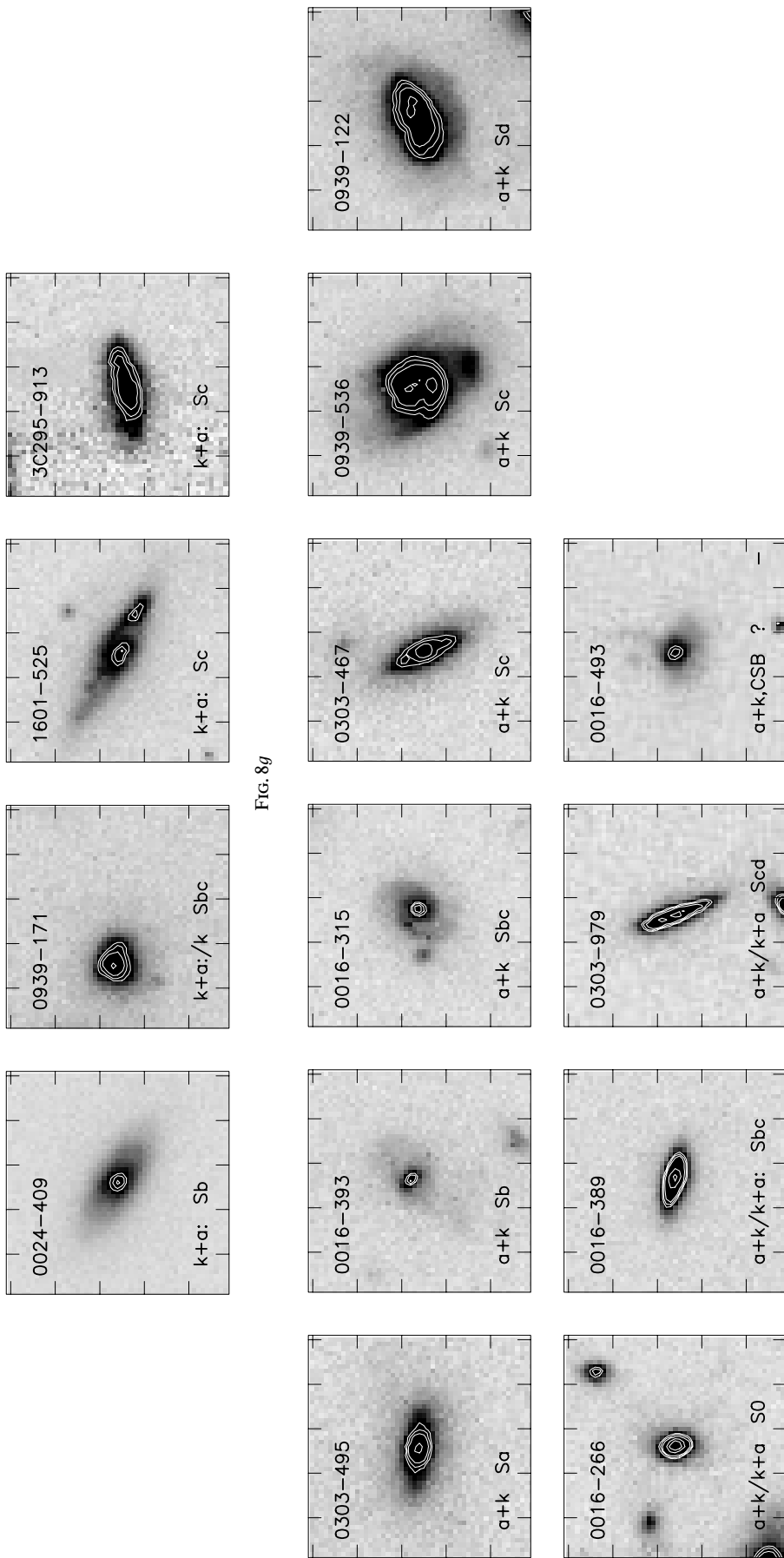


FIG. 8g

FIG. 8h

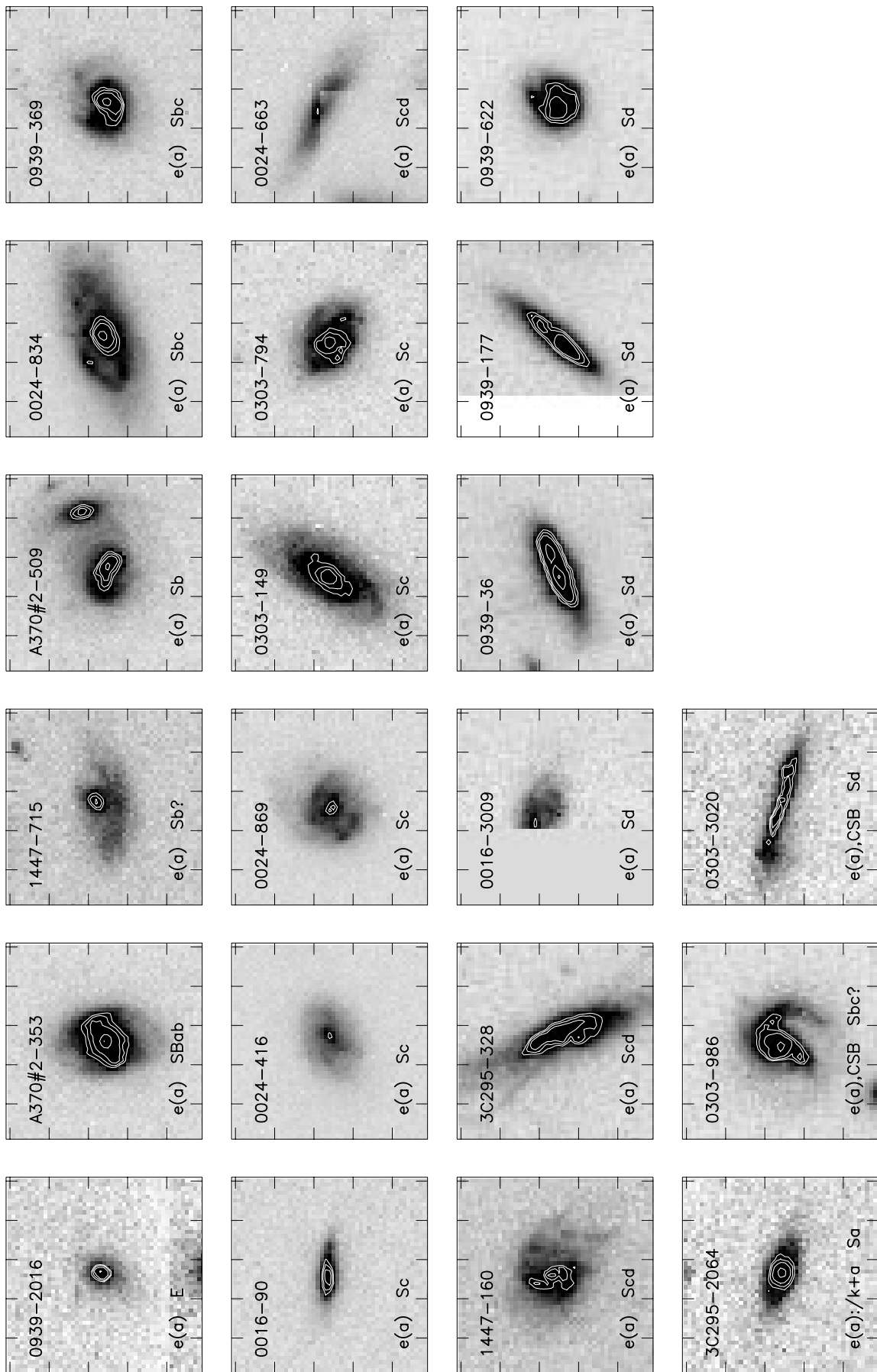


FIG. 8f

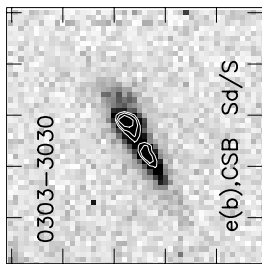
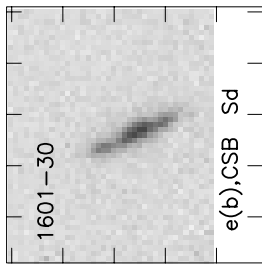
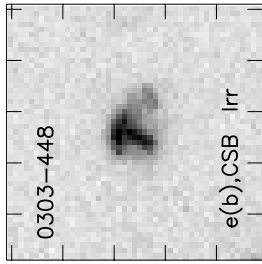
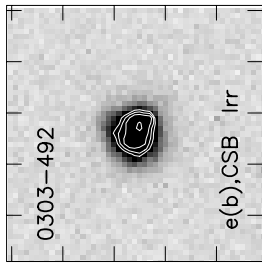
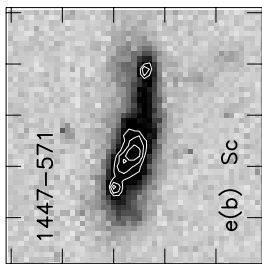
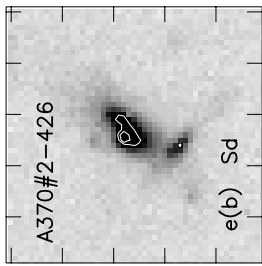
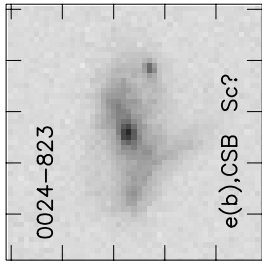
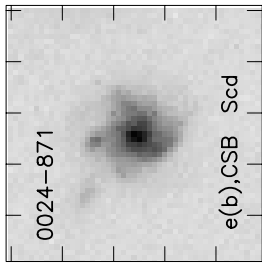
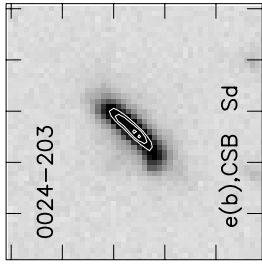
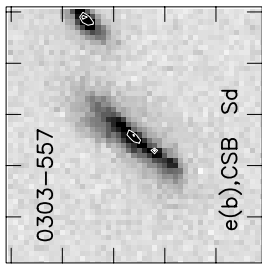


FIG. 8k

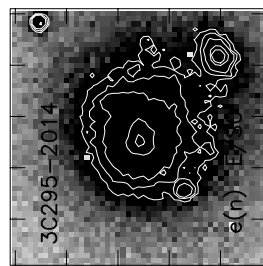
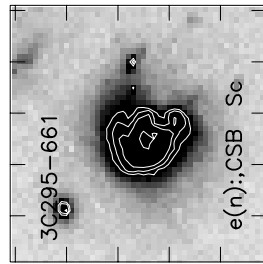
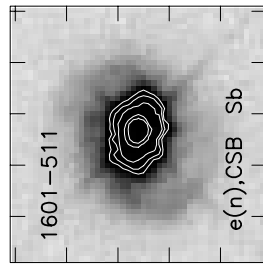
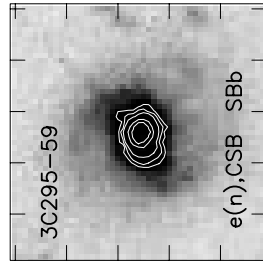


FIG. 8l

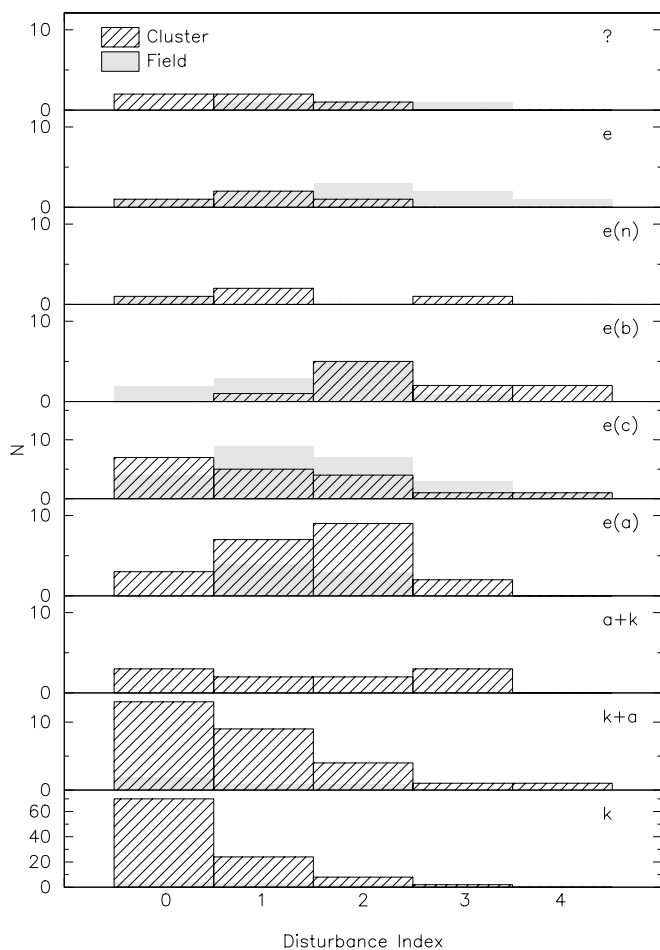


FIG. 9a

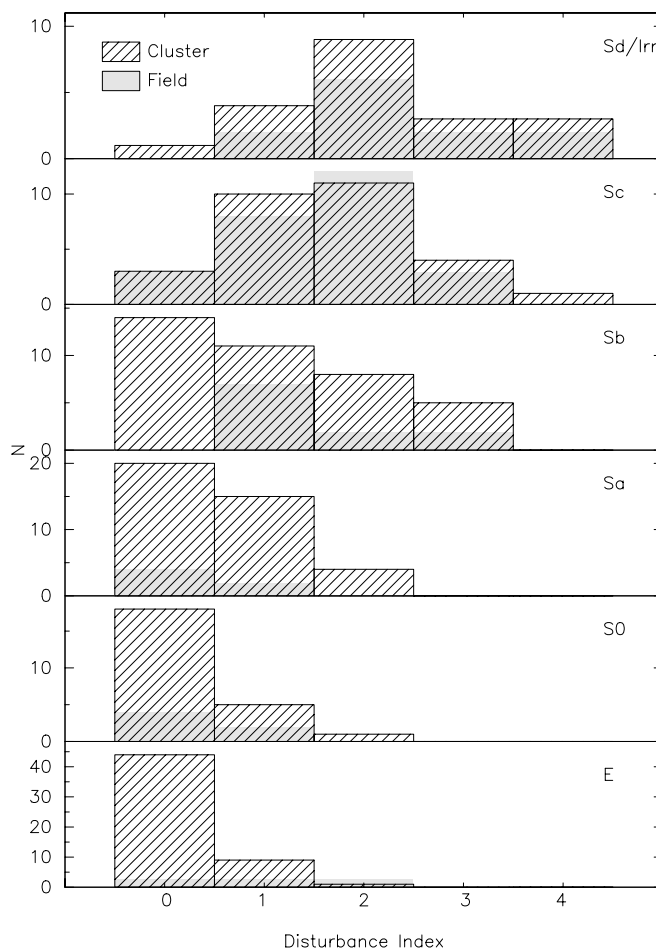


FIG. 9b

FIG. 9.—(a) Histograms indicating the distribution of spectral types within the different disturbance classes, D , for both cluster and field populations (hatched and filled histograms, respectively). $D \geq 2$ denotes strongly asymmetric or disturbed light distribution. (b) The numbers of galaxies in the different disturbance classes as a function of galaxy morphology. Note the broad similarity of the cluster and field distributions for the later type spiral galaxies.

spirals. The $k+a/a+k$ class does include some elliptical galaxies, but the majority are disk galaxies, a few of which have an irregular or disturbed appearance. The significance of the correlation of morphology and spectral class are discussed further in P99.

We briefly discuss evidence for interactions and mergers on the spectral classes of galaxies in our cluster samples. (We also comment on this issue in § 5.2, which deals with the kinematics of the different cluster populations.) We show in Figure 9a below the distribution of disturbance class within the different spectral classes. The image disturbance, D , is a visual classification of the degree to which the galaxy's structure appears distorted or disturbed (S97) compared with a typical low-redshift galaxy of the same morphological type. The D class correlates well with the asymmetry of the galaxy's light profile (S97). Figure 9a suggests that the spectral properties of the galaxies broadly correlate with the degree of image distortion and disturbance, the active and recently active populations having more galaxies classed as strongly asymmetric or distorted. However, looking at Figure 9b we see an arguably stronger correlation between morphology and D with a pronounced shift toward higher D values in going to later types (Sb–Sd/Irr), which may, in fact, be responsible for the correlation seen in Figure 9a. These trends could be due to a failure on our part

to actually separate disturbance from a natural trend toward more irregular morphology for late-type systems, but the large number of $D \geq 2$ Sc galaxies (a type that is generally symmetric for low-redshift galaxies) suggests that the effect is real.¹³ If so, it most likely reflects the greater fragility of disks (compared with bulges) to perturbations, and the greater frequency of perturbations at higher redshift. However, we see that this effect does not appear to be result of the high-density cluster environment: Figure 9b shows that $50\% \pm 8\%$ of the cluster Sb–Sc–Sd/Irr galaxies have $D \geq 2$, a proportion similar to that seen in the late-type field population, $60\% \pm 11\%$. The same lack of correlation of disturbance with environment is seen at low-redshift (Hashimoto & Oemler 1999).

4.4. Spectroscopic Properties of the Cluster Galaxies

In Figure 10 we quantify the distribution of morphological type for the various spectral classes, for both cluster members and field galaxies. The strong, although broad, relation between morphology and star formation seen in low-redshift galaxies is present in this intermediate redshift

¹³ This tendency of intermediate-redshift disk galaxies to appear more asymmetric than low-redshift galaxies of similar type has been reported in essentially all studies of this type.

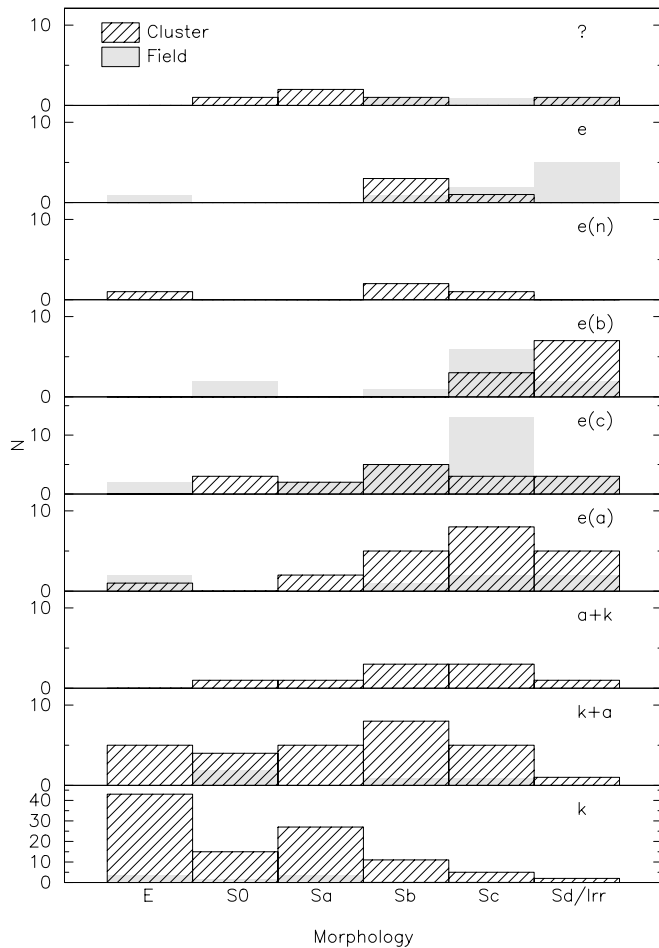


FIG. 10.—Comparison of the distribution of morphological type within each spectroscopic class for both cluster and field galaxies.

sample as well. Looking at the star-forming population that causes the Butcher-Oemler effect we see a clear tendency for these galaxies to be predominantly late-type systems (Couch et al. 1994; C98; Dressler et al. 1994; Oemler et al. 1997), although here there is a tail of earlier types (at least in the e(a) and e(c) classes). These active early-type (E and S0) galaxies comprise a higher fraction of the field population than they do in the clusters. The two “recently active” classes, $k+a$ and $a+k$, appear to have morphological distributions that are intermediate between the passive and active cluster populations. There seems to be a clear distinction between $k+a$ and $a+k$ in the sense that the latter are of later morphological type, although the small number of $a+k$ types limits the statistical certainty of this result.

It is interesting that, although the passive cluster population is dominated by elliptical and S0 galaxies, there is a significant number of later types, stretching out to Sd/Irr, which also show no emission lines. Aperture biases in our spectroscopy are unlikely to explain the lack of observed star formation in this group: the spectra sample the central $\sim 65 h^{-2} \text{ kpc}^2$ of these distant galaxies. Further support for a lack of ongoing star formation in these systems is shown by the uniform red colors of those galaxies for which we have imaging in two passbands with WFPC2.¹⁴

¹⁴ It should be noted that according to our definitions, an integrated spectrum of M31 would place it in the k class.

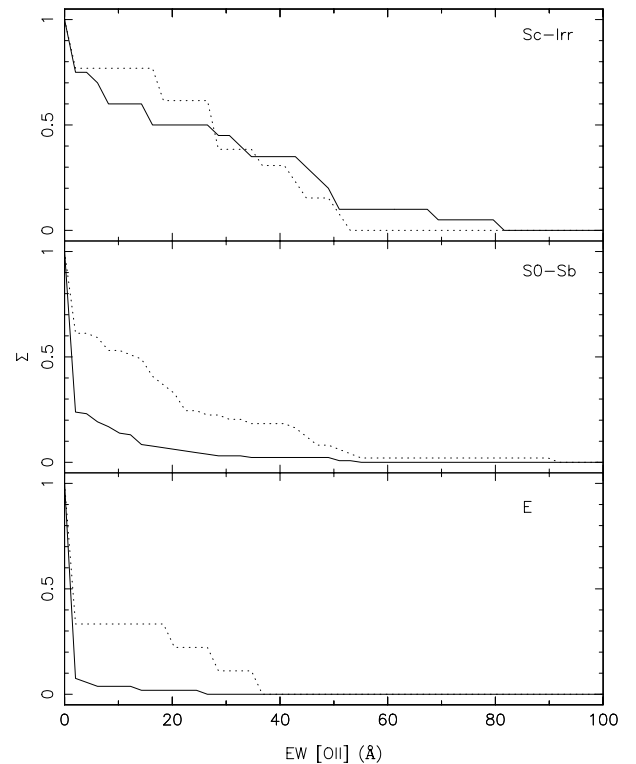


FIG. 11.—Cumulative distribution of the $[\text{O II}]$ 3727 EW for three independent morphological bins for both cluster (solid line) and field (dotted line) populations.

We quantify the occurrence of passive late-type galaxies, and compare cluster and field populations, in Figure 11. Using the cumulative distribution of $[\text{O II}]$ 3727 EW, we find that for the morphological groups E and S0–Sb there is a significantly higher fraction of galaxies showing little or no $[\text{O II}]$ emission in clusters as compared with the field. The likelihood, P , that the cluster and field samples are drawn from the same population is less than $\log_{10} P < -2.4$ for both E and S0–Sb samples. However, the comparison of the $[\text{O II}]$ distribution of the latest type systems (Sc–Irr, $T = 7\text{--}10$) shows no significant difference between the cluster and field, although the number of galaxies is somewhat smaller.

As an overall trend, then, there seems to be a decline in current star formation at a fixed Hubble-type from field to cluster (see also Balogh et al. 1998). Furthermore, based on $[\text{O II}]$ EW alone as a measure of star formation, we see no evidence for enhanced star formation in late-type cluster galaxies compared with the equivalent morphological sample in the field. We discuss this incidence of passive late-type galaxies further in P99.

In contrast to these results based on $[\text{O II}]$ EW, the distribution of D4000 strengths (Fig. 12) is very similar for cluster and field: the individual morphological types are indistinguishable in D4000 at better than $\log_{10} P > -1$ in each case. Thus, while $[\text{O II}]$, the tracer of current star formation, shows a decline in the cluster, this does not appear to be reflected in an index sensitive to the star formation averaged over a somewhat longer period of the recent past ($\sim 1\text{--}3$ Gyr).

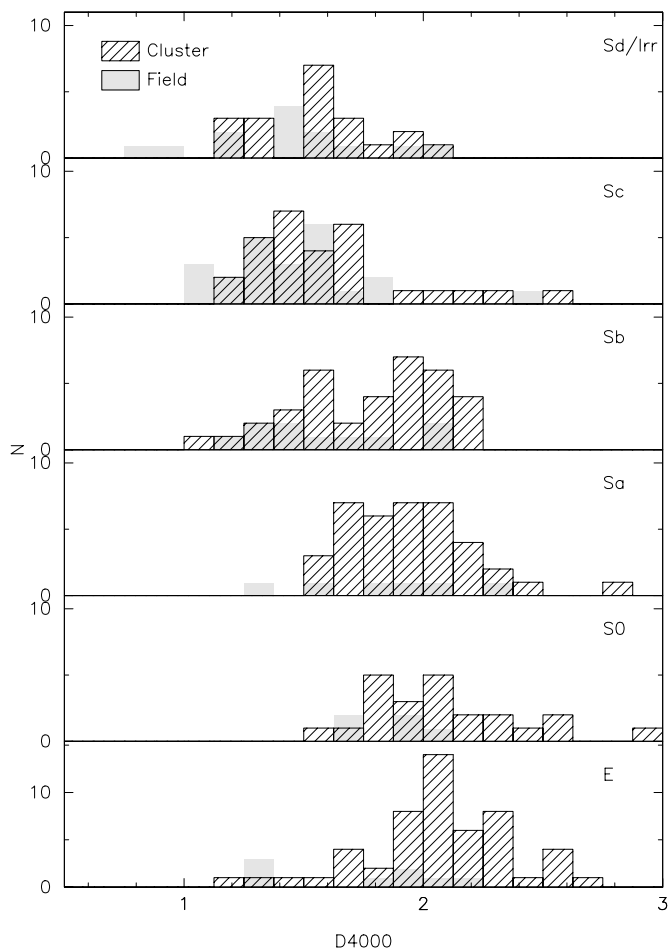


FIG. 12.—Comparison of the distribution of D4000 measures in the different morphological types for both cluster and field galaxies.

5. RESULTS AND DISCUSSION

5.1. The Incidence of $k + a/a + k$ and $e(a)$ Galaxies

Our spectral catalog exhibits one effect that is especially strong: the incidence of $k + a/a + k$ galaxies in distant clusters is very high compared with the surrounding field. Table 7 shows that in the cluster sample we have 60 examples of $k + a$ and 18 examples of $a + k$, totaling 18% of the sample. This is similar to the typical value of $\sim 10\%$ – 20% found by magnitude-limited surveys of distant clusters (DG92; C98). However, this value strongly contrasts with the seven occurrences, all $k + a$, found in the high-redshift field sample, only 2%.

Indeed, four of these seven cases are either uncertain or borderline, a far greater fraction than for the cluster sample, so an incidence of $\sim 1\%$ is compatible with these data. For the low-redshift Las Campanas Redshift Survey (hereafter LCRS), Zabludoff et al. (1996) found an incidence of 0.2%, but their selection criteria included a stronger limit on $H\delta$ of 5.5 \AA and they note that the number increases to 0.6% when the limit is dropped to 4.5 \AA . Y. Hashimoto (1998, private communication) has evaluated the occurrence of the spectral classes as defined in this paper for the LCRS and finds 2.3% for the occurrence of $k + a/a + k$ types. In summary, these data seem to point to *at most* a factor two increase in the frequency of $k + a/a + k$ types between the

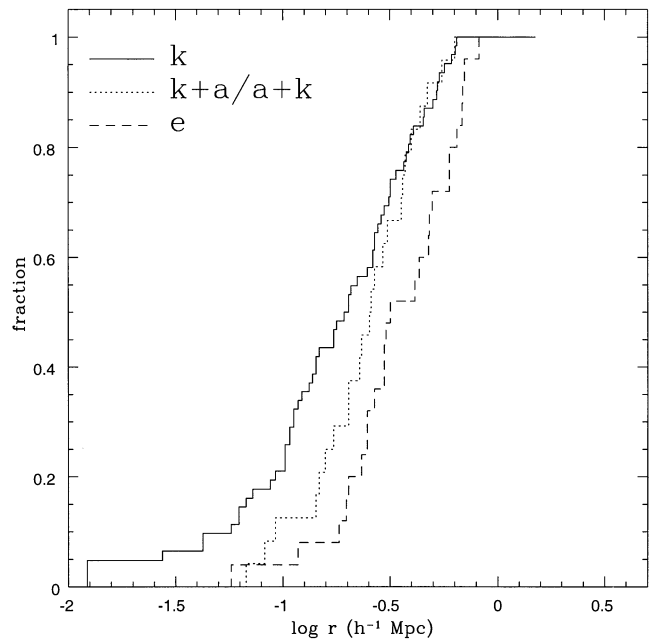


FIG. 13.—Cumulative radial distribution of different spectral types. These are shown for the all members from the whole sample that have $M_V < -19 + 5 \log_{10} h$. There is a clear difference between the radial distribution of k , $k + a/a + k$, and e -type galaxies, with the former being most concentrated and the latter the least. The $k + a/a + k$ class seems to be intermediate between the two, showing a similar decline to the k types on the outskirts of the cluster but a flatter distribution in the core, which is more in keeping with that seen for the e types.

low- and intermediate-redshift field populations. This is in marked contrast to the order-of-magnitude increase in the frequency of $k + a$ types in rich clusters. At low redshift, this frequency is $\lesssim 1\%$ (determined using the Dressler & Shectman 1988 catalog), compared with the 18% found here for the $z \sim 0.5$ clusters.¹⁵

Zabludoff et al. attributed many of the low-redshift field “E + A’s” as due to mergers and strong interactions, since morphologies of this type are often observed in the low-redshift examples. The expected evolution can be estimated from the change in the incidence of close pairs (Zepf & Koo 1989; Patton et al. 1997), which would be predicted to be the parent population. Patton et al. (1997) claim that the proportion of close pairs (two galaxies within $20 h^{-1} \text{ kpc}$) increases by a factor of ~ 1.5 between $z = 0$ and 0.33. Extrapolating this behavior to $\langle z \rangle = 0.42$ would predict an increase in the fraction of close pairs of ~ 2 – 3 over that seen locally. Although we see at most a factor of two increase in the $k + a$ population from low to high redshift using the LCRS and our field sample, this does not rule out that a significant fraction of field $k + a$ ’s are due to such mergers.

Zabludoff et al. argue further that, as the merger/interaction mechanism appears to be responsible for low-redshift field examples of such galaxies, it is reasonable to

¹⁵ Caldwell & Rose (1997) have reported a frequency of $\sim 15\%$ of notably stronger Balmer lines in early-type galaxies in five low-redshift clusters. These are for the most part lower luminosity systems with $H\delta < 3.0 \text{ \AA}$, which the authors suggest are the remnants of earlier bursts. The results of that study do not, therefore, conflict with the much lower frequency found by Dressler & Shectman for stronger, more luminous systems.

conclude that mergers may also be responsible for the $k+a/a+k$ galaxies in the intermediate-redshift clusters. However, the radically different evolution described above of the $k+a/a+k$ population between cluster and field environments suggests that the cluster environment is crucial in either the formation of *cluster* $k+a/a+k$ galaxies, or in prolonging their visibility. This could in part be due to an increased propensity for mergers in the groups infalling into the intermediate-redshift clusters. However, our morphological analysis (S97) finds only a minority of cases of $k+a$ spectra where the galaxy shows signs of a classic two-body merger, as Zabludoff et al. found for the low-redshift field examples. We conclude, then, that at least one mechanism other than mergers is responsible for the large fraction of $k+a/a+k$ galaxies in intermediate-redshift clusters.

As we discuss in P99, the majority of $k+a/a+k$ spectra are the result of a sudden decline in the rate of star formation that followed a substantial rise, or burst, of star formation, leaving a population of A stars to dominate the light for $\sim 10^9$ yr. Given the generic nature of the star formation history required to form an $a+k/k+a$, mergers are obviously not a unique explanation for the $k+a/a+k$ phenomena. For example, accretion of smaller satellites, instead of mergers of comparable mass systems, is not inconsistent with the morphologies we see.

5.2. The Distribution and Kinematic Properties of the Cluster Galaxies

As a final exercise in the comparison of spectroscopic properties with other cluster characteristics, we examine the radial distributions of our cluster sample as a function of spectroscopic type. We begin by assigning field centers: these positions are given in Table 2. There is usually little ambiguity in this because of the presence of a D or cD galaxy; these have been confirmed as the cluster centers in all cases from our the weak lensing analysis in Smail et al. (1997b). Even in more complex cases, such as Cl 1447+26, the ambiguity in choosing a center will play little role over the large range in radius we investigate.

In Figure 13 we show for the combined clusters the cumulative radial distribution for different spectroscopic types. This procedure is crude because it averages over the nonspherical distribution of galaxies within the clusters, but it may provide some insight into the characteristic distributions of different classes of galaxies. Not surprisingly, the k types, generally made up of E and S0 galaxies (Fig. 10), but including significant early-type spirals as well, are the most concentrated population in these clusters (see also S97). Also, not surprisingly, the emission line galaxies strongly avoid the center ($r \leq 50 h^{-1}$ kpc) of these clusters and have

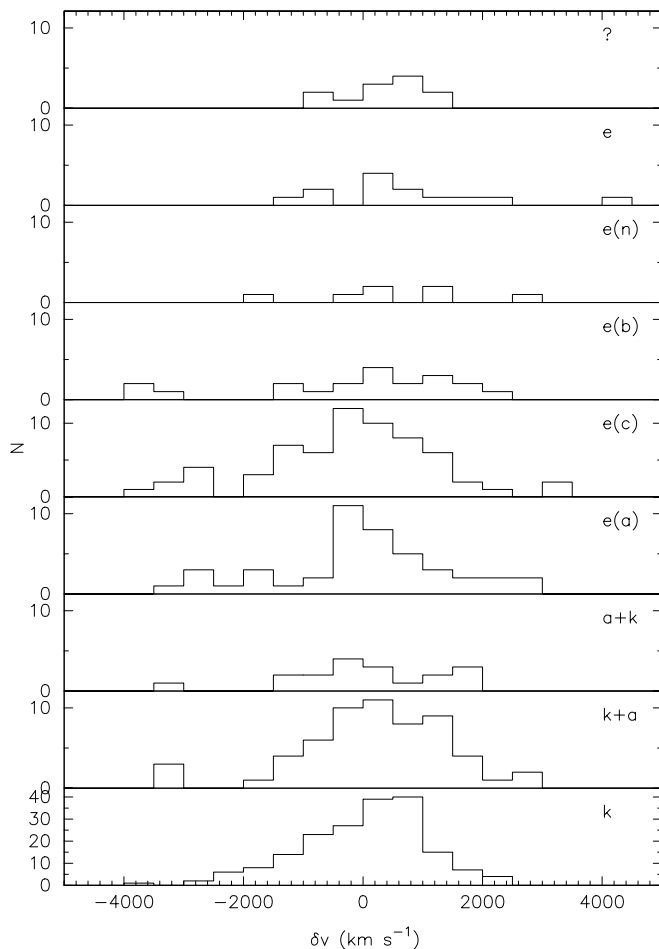


FIG. 14a

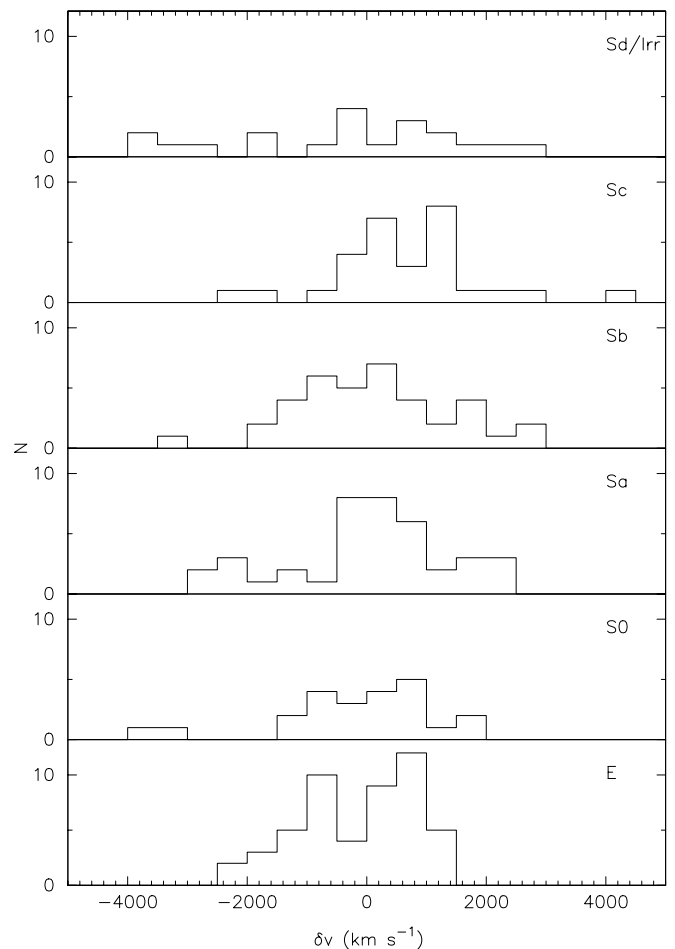


FIG. 14b

FIG. 14.—(a) The rest frame velocities of cluster members calculated relative to their respective cluster means (Table 2). These histograms are shown for the different spectroscopic classes. No scaling has been applied when combining the distributions from different clusters. (b) The rest frame velocities of cluster members relative to their respective cluster means. These histograms are shown for the different morphological types.

a much more extended distribution. What is perhaps more interesting is the way the $k + a/a + k$ types, which may sensibly interpreted as poststarburst galaxies, avoid the centers in contrast to the k types but are far less extended than the emission-line galaxies.¹⁶ The near absence of $k + a$ types in the field, discussed above, coupled with the sudden rise in their frequency as the cluster center is approached, with an almost complete demise in the central regions, appears to be clear evidence for the environment effecting either their formation or visibility.

We note in passing that a similar diagram subdividing the e types into $e(a)$, $e(c)$, and $e(b)$ shows no significant difference, although there is a hint that the $e(a)$ class has a slightly more extended distribution.

We now investigate the rudimentary kinematics of the sample of cluster members. In Table 8 we list the rest frame velocity dispersions and uncertainties for the entire cluster sample broken down in terms of morphological type, spectral class, disturbance and activity class (the latter three sections refer only to those galaxies lying within the WFPC2 fields). The distributions for the spectral and morphological types are also shown in Figure 14. These values are calculated using the mean cluster redshifts listed in Table 2 and are simple averages across the cluster (no allowance has been made for different velocity dispersion for the different clusters: when such corrections are applied they make no qualitative change to the conclusions listed below). The uncertainties in the velocity dispersions are 1σ values estimated from bootstrap resampling of the observed distributions.

Starting with the morphological samples in Table 8 we see a marked difference between the velocity dispersion of the elliptical galaxies and all the later types, the latter having higher dispersions (including the S0 galaxies). A similar difference is noticeable when the sample is split into different spectral classes (now including the whole spectroscopic catalog of members). Interestingly, the galaxies whose spectra were too poor to be classified, the “?” class, show the lowest dispersion: suggesting that these may be predominantly passive, cluster galaxies.

The strongest trend is the significantly higher velocity dispersion of the presently or recently star-forming systems compared with the passive population (see Dressler 1986). In particular, combining the different spectral classes ($e(\text{all})$ comprises $e(a)/e(b)/e(c)/e(n)/e$) from Table 8 we find that the emission-line and k -type galaxies have relative dispersions of $\sigma_{\text{em}}/\sigma_k = 1.40 \pm 0.16$, with the $k + a/a + k$ galaxies being intermediate between the two. The higher dispersions of the active populations are consistent with these galaxies being less virialized than the k -type population. Such a trend can also be discerned in the variation of velocity with activity (as traced by the $[\text{O II}]$ EW) *within* the individual morphological types. Splitting each of the more active morphological classes (Sb-Sd/Irr) at its median $[\text{O II}]$ EW into “low” and “high” activity samples we find the dispersions listed at the bottom of Table 8 for the different morphological samples. For all three morphological types, the more active sample shows the higher velocity dispersion, although the

¹⁶ It is tempting to describe this distribution as a “thick shell,” but we consider this to be potentially misleading because of the substantial departures from spherical symmetry exhibited by our clusters. Rather, it is probably more instructive to think of $k + a/a + k$ types occurring most frequently at an intermediate radius, $R \sim 200$ kpc.

TABLE 8
VELOCITY DISPERSIONS OF CLUSTER POPULATIONS

Sample	N	$\langle v \rangle$ (km s^{-1})	σ (km s^{-1})	$\delta\sigma$ (km s^{-1})
Morphological Types				
E	50	-109.9	974.9	78.7
S0	24	-378.7	1709.7	374.1
Sa	39	34.3	1336.5	137.2
Sb	38	179.5	1290.6	147.7
Sc	29	640.9	1212.6	219.2
Sd/Irr	20	-323.2	1894.6	231.9
Spectral Classes				
k	186	12.5	1064.8	55.2
$k + a$	60	105.4	1421.6	204.9
$a + k$	18	120.9	1236.4	223.7
$e(a)$	44	-27.2	1420.9	151.3
$e(c)$	64	-226.4	1437.1	126.2
$e(b)$	20	-168.8	1740.1	260.9
$e(n)$	7	576.1	1495.3	404.9
e	13	743.2	1400.1	288.8
?	12	367.6	694.1	116.3
k	186	12.5	1064.8	55.2
$k + a/a + k$	78	109.0	1373.4	172.4
$e(\text{all})$	148	-36.3	1486.0	90.1
Disturbance Classes				
$D = 0$	100	-33.9	1252.9	144.9
$D = 1$	54	207.6	1382.8	146.2
$D = 2$	34	58.9	1417.5	202.3
$D = 3$	12	307.5	1572.1	329.4
$D = 4$	4	-681.9	2884.3	807.8
Activity Classes				
Sb-high	10	-176.8	1429.5	294.1
Sb-low	28	180.4	1265.5	173.6
Sc-high	14	971.7	1293.7	334.2
Sc-low	15	332.1	1084.2	246.1
Sd-high	10	-945.1	2274.5	332.7
Sd-low	10	-298.8	1243.1	238.1

effect is only statistically significant for the Sdm/Irr sample. A higher velocity dispersion is often taken as a sign of an infalling population, but, as we discuss below, including spatial information in our analysis shows only weak evidence for infall.

We note that the $[\text{O II}]$ EW distributions for these active cluster members do not show any enhanced activity over that seen in the surrounding field for any given morphological type (see § 4.2). Apparently, then, the observed correlation of velocity dispersion and activity (as measured by $[\text{O II}]$ EW) is not triggered by a mechanism that causes the higher rate of star formation because of the high relative velocities of the galaxies within the clusters (i.e., ram pressure-induced star formation). We suggest instead that the correlation between activity and velocity dispersion reflects a decline in star formation in the galaxies that runs in parallel with and is causally linked to their virialization within the clusters. In this regard we also mention the trend for more disturbed galaxies to have higher velocity dispersions, Table 8, a result which remains when we restrict the analysis to late-type galaxies, Sb-Irr.

We next combine the velocity and positional information

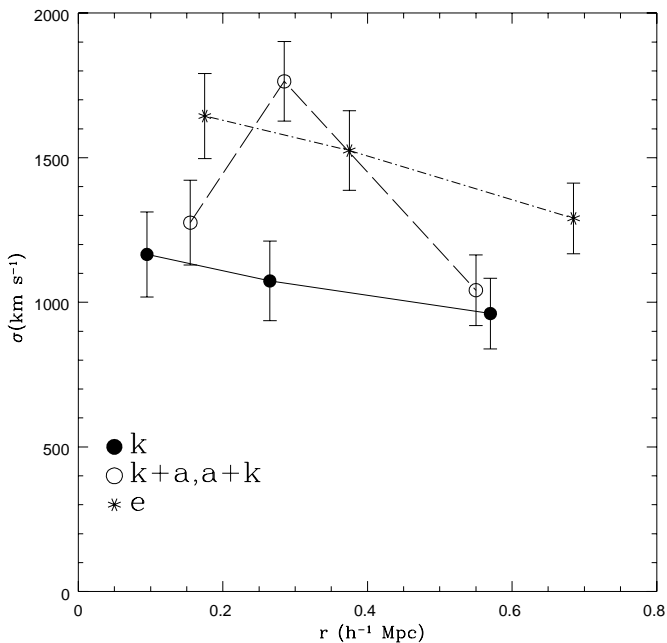


FIG. 15.—Velocity dispersions of the different spectral types averaged over the entire sample as a function of radius. The velocity dispersion is higher everywhere for active systems compared with passive galaxies. Note that the $k+a/a+k$ types exhibit a peak in velocity dispersion that may be related to their distinctive spatial distribution.

for the entire sample of clusters, focusing on the spectral classes, to calculate the velocity dispersion as a function of spectral class and radius. Dressler (1986) used the Giovanelli & Haynes (1983) catalog of spirals in nearby clusters to show that gas-poor spirals tend to travel on radial orbits that take them into the cluster center, as compared with the more isotropic orbits of the gas-rich spirals. Here we divide the k , $k+a/a+k$, and emission-line classes into three bins of radial position, each containing one-third of their respective samples. The resulting velocity dispersions are shown in Figure 15.

Unlike the clear difference in the orbital properties of gas-deficient systems in nearby clusters, our sample exhibits ambiguous evidence at best. The k and e types both have velocity dispersion that falls gently with radius or are, within the errors, flat. This suggests populations on mildly radial orbits, possibly an infalling population, or a simple isothermal distribution. More puzzling is higher velocity dispersion of the $k+a/a+k$ types (compared with the k types) in one of the three radial zones, which appears to be statistically significant. It is possible, of course, that higher velocities increase the chance of producing a $k+a/a+k$. It is also possible that this kinematic feature is connected with their unusual radial distribution, as mentioned above. A system of largely circular orbits that might characterize this distribution, which is concentrated like the k types but avoids the core, would appear to have a higher velocity dispersion because of projection of what are largely tangential velocities. This is, however, not consistent with

the idea that such galaxies derive from an infalling population on what are basically radial orbits. At this point, the statistics are poor enough, and the range of models so broad, that it is not worthwhile to explore this further here.

6. CONCLUSIONS

1. We have presented detailed spectroscopic observations of 657 galaxies in the fields of 10 $z = 0.37$ – 0.56 clusters. Combining these with our detailed *HST*-based morphological catalogs in these fields we construct samples of 204 cluster members and 71 field galaxies with both accurate spectral and morphological information.

2. Using observational and theoretical justifications we have constructed a new quantitative spectral classification scheme and use this to interpret correlations between our spectral information and other properties of the galaxies in our catalog.

3. Based on an analysis of the $[O\ II]$ EW distributions, we find no evidence for an increase in the occurrence of strongly star-forming galaxies in the moderate-redshift cluster environment compared with the moderate-redshift field using morphologically selected samples. However, we do find a large population of late-type cluster, but not field, galaxies that show little or no evidence of ongoing star formation.

4. This passive, late-type cluster population is related to our spectral classes $k+a/a+k$, both of which we interpret as indicative of poststarburst behavior. Galaxies with $k+a/a+k$ spectra are 1 order of magnitude more frequent in the cluster environment compared with the high-redshift field.

5. These $k+a/a+k$ galaxies avoid the central regions of the clusters, in contrast to the k types, but are also far less extended than the emission-line galaxies, and much less common in the field. This appears to be clear evidence for the environment effecting either their formation or visibility.

6. A detailed analysis of the spectroscopic and morphological information discussed here is presented in Poggianti et al. (1999).

We thank Ray Lucas at STScI for his enthusiastic help, which enabled the efficient gathering of these *HST* observations. BMP and HB warmly thank Steve Maddox for crucial help during the 1995 WHT run and in the subsequent reduction of those data. We also thank Alfonso Aragón-Salamanca, Nobuo Arimoto and Amy Barger for useful discussions and assistance. AD and AO acknowledge support from NASA through STScI grant 3857. IRS acknowledges support from a PPARC Advanced Fellowship and from Royal Society and Australian Research Grants while an Honorary Visiting Fellow at UNSW. WJC acknowledges support from the Australian Department of Industry, Science and Technology, the Australian Research Council and Sun Microsystems. This work was supported in part by the Formation and Evolution of Galaxies network set up by the European Commission under contract ERB FMRX-CT96-086 of its TMR program. We acknowledge the availability of the Kennicutt (1992) atlas of galaxies from the NDSS-DCA Astronomical Data Center.

REFERENCES

- Abraham, R., et al. 1996, ApJ, 471, 694
 Allington-Smith, J. R., et al. 1994, PASP, 106, 983
 Aragón-Salamanca, A., Ellis, R. S., Couch, W. J., & Carter, D. 1993, MNRAS, 262, 764
 Balogh, M. L., Schade, D., Morris, S. L., Yee, H. K. C., Carlberg, R. G., & Ellingson, E. 1998, ApJ, 504, L75
 Barger, A. J., Aragón-Salamanca, A., Ellis, R. S., Couch, W. J., Smail, I., & Sharples, R. M. 1996, MNRAS, 279, 1
 Barger, A. J., et al. 1998, ApJ, 501, 522
 Bothun, G. D., & Gregg, M. D. 1990, ApJ, 350, 73
 Butcher, H., & Oemler, A., Jr. 1978, ApJ, 279, 18
 ———. 1984, ApJ, 285, 426
 Caldwell, N., & Rose, J. A. 1997, AJ, 113, 492
 Couch, W. J., Barger, A. J., Smail, I., Ellis, R. S., Sharples, R. M., & Smail, I. 1998, ApJ, 497, 188 (C98)
 Couch, W. J., Ellis, R. S., Sharples, R. M., & Smail, I. 1994, ApJ, 430, 121
 Couch, W. J., & Sharples, R. M. 1987, MNRAS, 229, 423 (CS87)
 Dressler, A. 1986, in *Nearly Normal Galaxies*, ed. S. M. Faber (New York: Springer), 276
 Dressler, A., et al. 1997, ApJ, 490, 577
 Dressler, A., & Gunn, J. E. 1983, ApJ, 270, 7
 ———. 1992, ApJS, 70, 1 (DG92)
 Dressler, A., Oemler, A., Jr., Butcher, H., & Gunn, J. E. 1994, ApJ, 430, 107
 Dressler, A., & Shectman, S. A. 1987, AJ, 94, 899
 ———. 1988, AJ, 95, 284
 Ellis, R. S., Smail, I., Dressler, A., Couch, W. J., Oemler, A., Butcher, H., & Sharples, R. M. 1997, ApJ, 483, 582
 Fisher, D., Fabricant, D., Franx, M., & van Dokkum, P. 1998, ApJ, 498, 195
 Franx, M. 1993, ApJ, 407, L5
 Giovanelli, R., & Haynes, M. 1983, AJ, 88, 881
 Hashimoto, Y., & Oemler, A., Jr. 1999, in preparation
 Kells, W., Dressler, A., Sivaramakrishnan, A., Carr, D., Koch, E., Epps, H., Hilyard D., & Pardeilan, G. 1999, PASP, 110, 1487
 Kennicutt, R. C., Jr. 1992, ApJS, 79, 255
 Lavery, R. J., & Henry, J. P. 1994, ApJ, 426, 524
 Lubin, L. M. 1996, AJ, 112, 23
 Oemler, A., Dressler, A., & Butcher, H. R. 1997, ApJ, 474, 561
 Patton, D. R., Pritchet, C. J., Yee, H. K. C., Ellingson, E., & Carlberg, R. G. 1997, ApJ, 475, 29
 Poggianti, B. M., Smail, I., Dressler, A., Couch, W. J., Barger, A. J., Butcher, H., Ellis, R. S., & Oemler, A., Jr. 1999, 518, in press (P99)
 Rakos, K. D., Odell, A. P., & Schombert, J. M. 1997, ApJ, 490, 194
 Rakos, K. D., & Schombert, J. M. 1995, ApJ, 439, 47
 Smail, I., Dressler, A., Couch, W. J., Ellis, R. S., Oemler, A., Jr., Butcher, H., & Sharples, R. M. 1997a, ApJS, 110, 213 (S97)
 Smail, I., Edge, A. C., Ellis, R. S., & Blandford, R. D. 1998, MNRAS, 293, 124
 Smail, I., Ellis, R. S., Dressler, A., Couch, W. J., Oemler, A., Jr., Butcher, H., & Sharples, R. M. 1997b, ApJ, 479, 70
 Stanford, S. A., Eisenhardt, P. R., & Dickinson, M. E. 1995, ApJ, 450, 512
 ———. 1998, ApJ, 492, 461
 Zabludoff, A. I., Zaritsky, D., Lin, H., Tucker, D., Hashimoto, Y., Shectman, S. A., Oemler, A., Jr., & Kirshner, R. P. 1996, ApJ, 466, 104
 Zepf, S. E., & Koo, D. C. 1989, ApJ, 337, 34
 Zijlstra, A., Giraud, E., Melnick, J., Dekker, H., & D'Odorico, S. 1996, ESO Operating Manual v. 3.0 (Garching: ESO)